ACS OMEGA

http://pubs.acs.org/journal/acsodf

Article

Room-Temperature, Deep-Red/NIR-Emissive, C_3-Symmetric (n,π-conjugated) Columnar Liquid Crystals: C_{3h}-Tris(keto-hydrazone)s

Rashmi Ashwathama Nayak, Bhyranalyar Nagarajappa Veerabhadraswamy, Doddamane S. Shankar Rao, Achalkumar Ammathnadu Sudhakar, and Channabasaveshwar V. Yelamaggad*

Cite This: *ACS Omega* 2021, 6, 3291−3306

Read Online

ACCESS | Metrics & More | Article Recommendations | Supporting Information

ABSTRACT: The first examples of deep-red/near-infrared (NIR) photoluminescent, (n,π-conjugated) discotics, namely, C_{3h}-tris(keto-hydrazone)s, which are the tautomers of tris(azo-enol)s, have been synthesized via a facile one-step triple azo-coupling and characterized. The n,π-resonance-assisted intramolecular H-bonding, rendering planarity and shape persistence to the central core, facilitates their self-assembly into either a hexagonal columnar (Col_h) phase (*p6mm* lattice) or a columnar rectangular (Col_r) phase (*p2mm* lattice), over an extended thermal range including room temperature, fluorescing in the deep-red/NIR-I region. The low band gap with deep-red/NIR emission makes them ideal candidates for NIR-organic light-emitting diodes (OLEDs) and bioimaging.

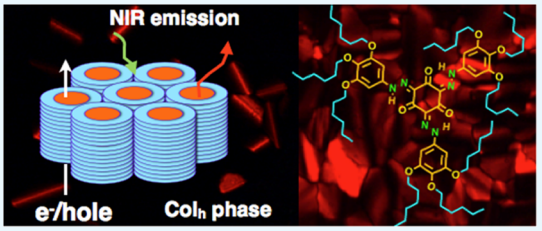

INTRODUCTION

The organic dye materials capable of absorbing and/or emitting light in the deep-red to near-infrared, 650−950 nm (NIR-I), regime are receiving significant attention owing to their exceptional properties that are finding applications in a wide range of high-technological endeavors.[1] Examples of these include bioimaging, organic photovoltaics (OPVs), dye-sensitized solar cells, organic light-emitting diodes (OLEDs), photonics, etc.[2,3] In practical terms, they have been fundamental, employed as active layers in electronic devices to account for vital processes such as light absorption/emission, carrier-injection or blocking, and electron−hole recombination or separation. Generally, the occurrence of long-range (extended) π-conjugation or n,π-conjugation in the basic organic structure enables them to address the processes mentioned above, including deep-red/NIR light emission. The organic dyes incorporating low-band-gap chromophores capable of emitting/absorbing light in most of the solar spectrum are the ideal candidates for OLEDs and solar cells.[4−6] Among a large variety of OLED structures reported hitherto, white OLEDs (WOLEDs) have received enormous attention owing to their exceptional characteristics such as high efficiency, fast switching, low energy consumption, wide viewing angle, flexibility, etc. The requisite white emissions in such devices are achieved generally by employing appropriate organic materials capable of emitting blue, red, and green light concurrently.[7] However, making white-light emitters is highly challenging, especially because red-emitting organic materials are lagging behind their blue and green counterparts in terms of efficiency. Here, the concern is that the lowering or even elimination of emission takes place due to the competition between nonradiative transition pathways and fluorescence relaxation.[8,9]

Incidentally, the aforesaid material characteristics and phenomenon occur in columnar (Col) liquid crystal (LC) phases, which comprise parallelly packed, indefinitely long columns arranged in two-dimensional (2D) lattices.[10,11] Each column stems from the self-assembly of disklike (discotic) mesogens (discogens) comprising a flat aromatic core substituted peripherally with several alkyl tails. The intense $\pi-\pi$ stacking of discotic molecules in each column creates a one-dimensional (1D) charge carrier pathway along the column axis, whereas, in contrast, the tails serve as an insulator.[10] Thus, Col LC phases, which are regarded as quasi 1D conductors or molecular wires, are highly promising because their electron/hole carrier mobilities and light-absorbing/-emitting properties are tunable via the rational designing and synthesis of a new discotic mesogen. Over the past two decades or so, our group has been working on this topic with an emphasis on the design and development of discotics capable of exhibiting both photophysical (absorption/emissive) behavior and conductive property. For instance, based on the exceptional physicochemical studies on tris(*N*-salicylideneaniline)s (TSANs) reported by MacLachlan and co-workers in 2003,[12] we have prepared a wide variety of discotic TSANs (**I**; Figure 1) and examined their thermal and

Received: November 27, 2020
Accepted: January 12, 2021
Published: January 22, 2021

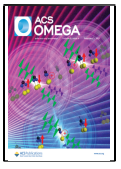

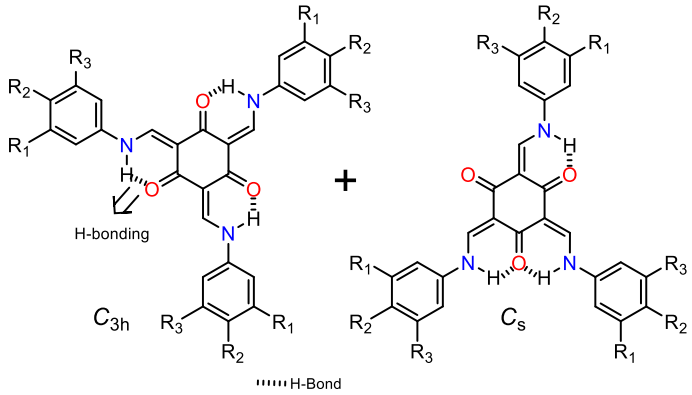

I : R = 3,4-(*n*-alkoxy)$_2$C$_6$H$_3$; R = 3,4,5-(*n*-alkoxy)$_3$C$_6$H$_2$

Previous work (refs. 13-19): Discotic tris(*N*-salicylideneaniline)s (**TSANs**). Exist in an Inseparable Mixture of C_{3h} & C_s Isomers. Properties: Columnar LC Behavaior & Fluorescence in Visible Region

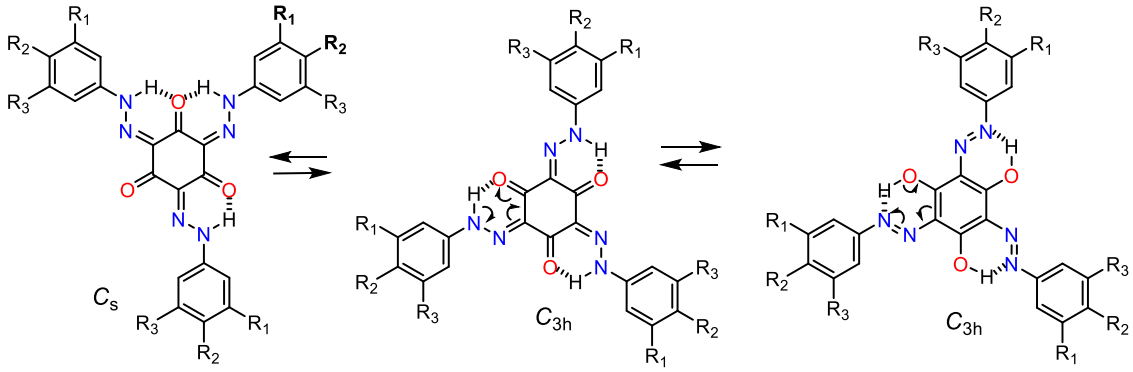

Tris(keto-hydrazone): THN-C_s **Tris(keto-hydrazone): THN-C_{3h}** **Tris(azo-enol): TAZ-C_{3h}**

Previous work reported by Lee *et al* (ref. 22): **II - THNs-C_{3h}** ; R_1 = R_3 =H; R_3 = *tert*-butyl

Present work : Tris(keto-hydrazone)s - **THNs**
THN-(6)n - Series: R_1 = R_2 = n-OC_nH_{2n+1}; R_3 = H; n = 6-12 or R_1 = R_2 = (3*S*)-3,7-dimethyloctyloxy
THN-(9)n - Series: R_1 = R_2 = R_3 = n-OC_nH_{2n+1}; n = 6-12 or R_1 = R_2 = R_3 = (3*S*)-3,7-dimethyloctyloxy

Figure 1. Molecular structures of previously investigated discotic tris(N-salicylideneaniline)s (TSANs) (ref 13−19) and the structurally analogous discotic liquid crystals, namely, tris(keto-hydrazone)s (THNs) investigated in the present study.

photophysical behaviors.[13−19] The accumulated experimental results suggest that disk-shaped TSANs have great potential to act as conductive and/or emissive layers due to their inherent Col LC property in conjunction with photoluminescence in the visible region. The systematic investigations on several star-shaped LCs also afforded similar results and conclusions.[20,21] These findings motivated us to search for new organic dyes that are structurally similar to TSANs but differ marginally in their composition.

Thus, structurally analogous motifs, namely, tris(keto-hydrazone)s (**THNs**) (**II**; Figure 1), which are the tautomers of tris(azo-enol)s (TAZs; Figure 1), reported by Lee et al.[22] caught our genuine attention while reviewing the literature. They demonstrated that these C_3-symmetric, n,π-conjugated systems exhibit promising optical properties stemming from the conformational switching. As shown in Figure 1, **THNs**, which are stabilized by resonance-assisted intramolecular H-bonding, can exist hypothetically in C_{3h} (**THN-C_{3h}**) and C_s (**THN-C_s**) geometric isomers, but it is the former core that was obtained in the pure form after the synthesis.[22] Thus, we were motivated to induce Col mesomorphism in this class of new dyes to disclose the unprecedented examples of LC THNs possibly. Particularly, to determine whether columnar liquid crystallinity could be induced in this novel class of materials, we projected to realize a number of disk-shaped tris-(hydrazone)s by varying the length and numbers of peripheral alkoxy tails on each of the three benzene cores attached to the central cyclohexane-1,3,5-trione. We report herein the facile synthesis and characterization of two series of Col LCs derived from the THN-core. The general molecular structures of the two series of compounds synthesized, each substituted peripherally with six and nine *n*-alkoxy tails, are presented in Figure 1. To investigate the correlation between the thermal properties and the structure, compounds of both series have been substituted with *n*-hexyloxy to *n*-dodecyloxy paraffinic tails and a chiral tail, namely, the 3,7-dimethyloctyloxy chain. For convenience, the tris(keto-hydrazone)s consisting of six and nine *n*-alkoxy/branched tails have been, respectively, abbreviated as **THN(6)n**/**THN(6)nB** and **THN(9)n**/**THN-(9)nB**, where the number in parenthesis represents the total number of peripheral alkoxy tails, while **n** indicates the number of carbon atoms present in each alkoxy tail and **B** signifies a

https://dx.doi.org/10.1021/acsomega.0c05779
ACS Omega 2021, 6, 3291−3306

Scheme 1. Synthesis of Discotic Tris(keto-hydrazone)s[a]

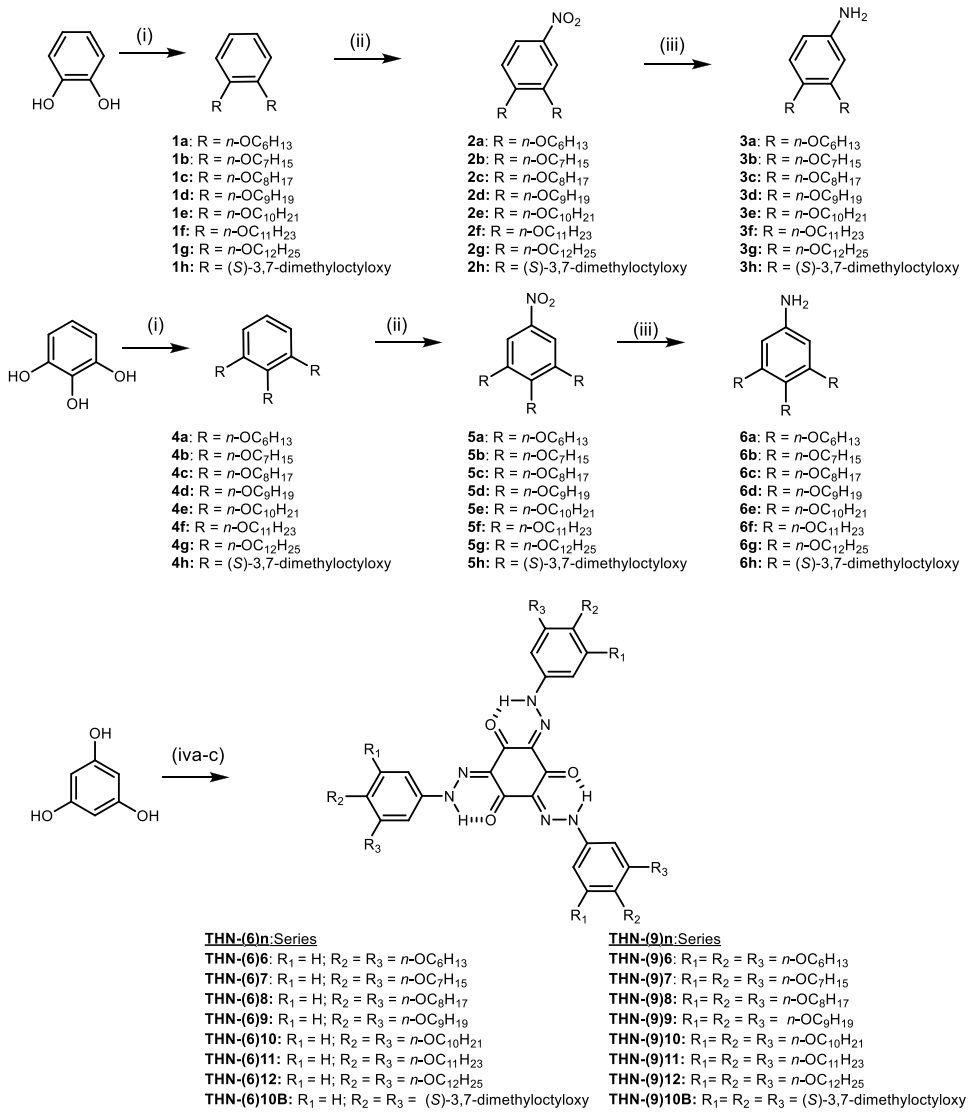

[a]Reagents and conditions: (i) *n*-bromoalkanes, anhyd. K_2CO_3, dimethylformamide (DMF), 80 °C, 12 h (52−85%); (ii) DCM, fuming HNO_3, $NaNO_2$, 0 to −5 °C, 15 min (53−78%); (iii) THF, Pd-C 10%, H_2 (1 atm, balloon), room-temperature (rt) (68−91%); (iv) (a) NaOH (2 M), methanol; (b) **3a−h**, HCl (2 M), methanol, $NaNO_2$, 0−5 °C; (c) **6a−h**, HCl (2 M), methanol, $NaNO_2$, 0−5 °C (48−60%).

branched chain. The detailed studies evidenced that these two new series of discotic dyes synthesized (Figure 1) show, besides redox behavior, deep-red/NIR photoluminescence (PL) in the entire thermal width of the Col phase, including room temperature, the first of its kind. This finding is notable given the fact that deep-red/NIR emission, thus far, has been observed in the solid state (thin film) or solutions of a few nondiscoid LCs[23−26] and triphenylene-based LCs.[27] In the sections that follow, we present the aforesaid experimental aspects and relevant details.

RESULTS AND DISCUSSION

Synthesis and Characterization. The synthesis of all target discotic tris(keto-hydrazone)s belonging to **THN(6)n** and **THN(9)n** series was carried out following Scheme 1. The synthesis of 3,4-bis(alkoxy)anilines (**3a−h**) was readily achieved, starting from catechol.[14−16] The Williamson etherification of catechol with various *n*-bromoalkanes, including (*S*)-3,7-dimethyl-1-bromooctane, afforded 1,2-bis(alkoxy)-benzenes (**1a−h**); these ethers were subjected to nitration using fuming nitric acid (HNO_3) in the presence of sodium nitrite ($NaNO_2$) in dichloromethane (DCM) to obtain 1,2-bis(alkoxy)-4-nitrobenzenes (**2a−h**). The catalytic hydrogenation of these nitro compounds at room temperature under 1 atm of H_2 (balloon) in the presence of 10% Pd/C (5 wt %) in tetrahydrofuran (THF) yielded the corresponding 3,4-bis(alkoxy)anilines (**3a−h**) in good yields. Similarly, other key intermediates, namely, 3,4,5-tris(alkoxy)anilines (**6a−h**), were prepared starting from pyrogallol.[14−16] It was subjected to *O*-alkylation with different *n*-bromoalkanes and (*S*)-3,7-dimethyl-1-bromooctane to obtain 1,2,3-tris(alkoxy)benzenes (**4a−h**). The nitration of compounds **4a−h** using fuming HNO_3 and $NaNO_2$ in DCM at low temperature afforded 1,2,3-tris(alkoxy)-5-nitrobenzenes (**5a−h**), which upon catalytic hydrogenation (H_2 balloon, 1 atm, 10% Pd/C) in THF gave the required anilines **6a−h** in good yields. In the final step, the triple azo-coupling reactions between phloroglucinol and aniline derivatives[22] (**3a−h** and **6a−h**) afforded the target

https://dx.doi.org/10.1021/acsomega.0c05779
ACS Omega 2021, 6, 3291−3306

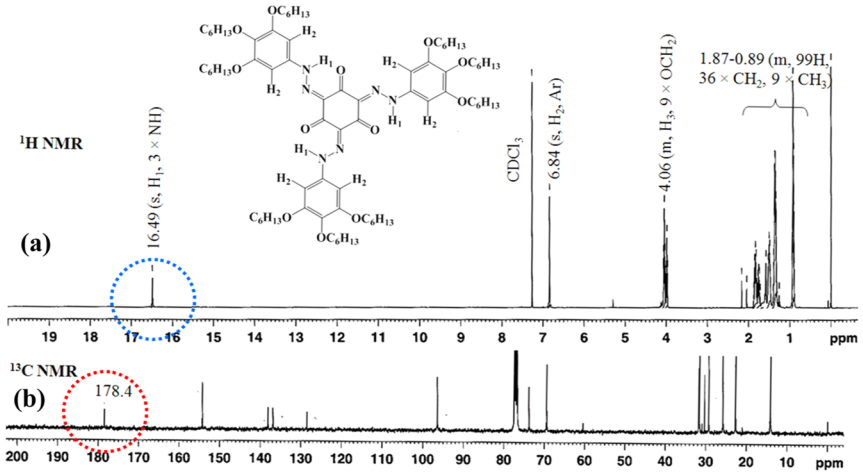

Figure 2. (a) ^{1}H NMR (400 MHz) and (b) ^{13}C NMR (100 MHz) spectra of **THN(9)6** in $CDCl_3$.

tris(keto-hydrazone)s of **THN(6)n** and **THN(9)n** series as bright-red solid or gummy (sticky) samples. The molecular structure and purity of the final materials belonging to **THN(6)n** and **THN(9)n** series were established by UV−vis, Fourier transform infrared (FTIR), ^{1}H and ^{13}C NMR spectroscopies, and elemental analyses. However, the structures and purity of the know intermediates were ascertained with the aid of FTIR and ^{1}H NMR spectroscopic techniques only. The characterization data of all of the discotics and intermediates realized were found to be consistent with the proposed structures. The details of synthetic protocols and characterization are given in the Experimental Section of the Supporting Information (SI); ^{1}H and ^{13}C NMR spectra are shown in Figures S1−S44.

The ^{1}H NMR spectra of all of the discotics belonging to **THN(6)n** and **THN(9)n** series, acquired in $CDCl_3$ at room temperature, show virtually identical patterns, except for the aromatic region (7−9 ppm) as expected (Figures S1−S44). The spectral patterns were found to be extremely simple, indubitably confirming their existence in high molecular symmetry. As a representative case, the ^{1}H NMR spectrum of tris(keto-hydrazone) **THN(9)6** recorded in $CDCl_3$ at 28 °C is shown in Figure 2a. It is immediately apparent from the spectrum that the protons of three −NH− groups around the central core resonate as a sharp singlet at ∼16.5 ppm (see the blue circle in Figure 2a). This remarkable down-field shift of the peak suggests the involvement of −NH− protons in the intramolecular H-bonding. It may be recalled here that a similar peak at ∼16.5 ppm was seen for −NH− protons of analogous motifs studied by Lee et al.[22] This clearly suggests the higher rotational symmetry of the compounds realized. That is, the pattern evidences their occurrence in the tris(keto-hydrazone) form having threefold (C_{3h}) rotational symmetry. The conclusion that these motifs exist in the C_{3h}-tris(keto-hydrazone) form was substantiated based on the ^{13}C NMR spectra; a distinct carbon resonance peak seen at ∼178 ppm is indicative of carbonyl carbon (=C = O) rather than phenolic (=CH-OH) carbon. The mentioned feature can be visualized in Figure 2b (see red circle marking), where the ^{13}C spectrum recorded in $CDCl_3$ at 28 °C for the tris(keto-hydrazone) **THN(9)6** is depicted. The thermal stability of the new discotics synthesized was evaluated by thermogravimetric analysis (TGA) at a rate of 10 °C min^{-1} under an inert atmosphere. The TGA data obtained for **THN(6)6** and **THN(9)6**, as representative cases, suggest that the compounds are stable up to 260 °C (Figure S45).

Evaluation of Mesomorphic Behavior. The thermal behavior of the newly synthesized C_{3h}-tris(keto-hydrazone)s was generally studied by a combination of optical microscopy (POM), differential scanning calorimetry (DSC), and X-ray diffraction (XRD). However, the mesomorphic behavior of the tris(hydrazone)s belonging to **THN(9)n** (trialkoxy) series could be determined with the aid of POM and XRD studies only as none of the members displayed any thermal events (signatures/peaks) in the DSC profiles. This is especially unexpected given the fact that the phase sequences and transition temperatures were highly reproducible under microscopic examination, suggesting that the mesogens of **THN(9)n** series are heat-resistant, meaning that their response to heat is slow. To determine the transition temperatures and phase type by POM, clean, untreated glass substrates were employed. During the preliminary evaluation using hot-stage microscopy, all of the discogens confirmed their liquid crystal behavior by exhibiting a combination of fluidity (shearability) and birefringence, as expected. The phase-transition temperatures determined by DSC (heating−cooling) traces of discogens of **THN(6)n** series were found to be in concurrence with those obtained from POM studies. Table 1 shows the thermal data along with the phase sequence of all of the discogens of both the series synthesized. The transition temperatures derived from peak temperatures in the DSC traces recorded during the first heating−cooling runs at a rate of 5 °C min^{-1} are presented for the **THN(6)n** series of tris(hydrazone)s. However, for the **THN(9)n** series of discotics, the transition temperatures noted during the optical study are given. Figure 3 depicts two horizontal bar graphs representing the phase sequence and transition temperatures recorded on their first heating.

All eight compounds of the **THN(6)n** series show qualitatively similar LC behavior. Of special significance, the discogen **THN(6)10** with branched peripheral tails shows mesomorphism at room temperature, unlike other members of the series. On cooling from the isotropic liquid, the discotic **THN(6)6** shows a Col phase at 125.3 (ΔH = 1.4 kJ mol^{-1}), manifesting optically in the form of rectilinear birefringent defects and homeotropic regions (Figure 4a inset); the presence of the latter pattern confirms the uniaxial nature of the phase.[28] It may be mentioned here that some members of

https://dx.doi.org/10.1021/acsomega.0c05779
ACS Omega 2021, 6, 3291−3306

Table 1. Phase Sequences and Transition Temperatures (°C)[a,b] of Tris(keto-hydrazone)s Belonging to THN(6)n and THN(9)n Series[f]

compound	phase sequence	
	heating	cooling
THN(6)6	Cr 119.6 (25.5) $Col_h/p6mm$ 125.3 (1.4) I	I 120 (1.4) $Col_h/p6mm$[c]
THN(6)7	Cr 105 (30.7) $Col_h/p6mm$ 152 (1.7) I	I 149 (1.6) $Col_h/p6mm$[c]
THN(6)8	Cr 96.7 (50.4) $Col_h/p6mm$ 152.9 (2.2) I	I 150.8 (1.8) $Col_h/p6mm$ 45.7 (24.1) Cr
THN(6)9	Cr 91.2 (34) $Col_h/p6mm$ 154.3 (2.1) I	I 153.8 (2) $Col_h/p6mm$ 52.1 (32.4) Cr
THN(6)10	Cr 94.4 (56.7) $Col_h/p6mm$ 149.2 (2.4) I	I 146.3 (2.2) $Col_h/p6mm$ 56.8 (7.8) Cr
THN(6)11	Cr 98.7 (47) $Col_h/p6mm$ 161.6 (2.9) I	I 159.5 (2.8) $Col_h/p6mm$ 62.6 (46) Cr
THN(6)12	Cr 92.5 (19.2) $Col_h/p6mm$ 156.8 (2.6) I	I 155.5 (2.5) $Col_h/p6mm$ 62.2 (18.1)
THN(6)10B	$Col_h/p6mm$ 131.2 (1.8) I	I 126.6 (1.8) $Col_h/p6mm$[e]
THN(9)6	$Col_h/p6mm$ 225 I[d]	I 218[d] $Col_h/p6mm$[e]
THN(9)7	Col 215 I[d]	I 211.7[d] $Col_r/p2mm$[e]
THN(9)8	$Col_r/p2mm$ 210 I[d]	I 205[d] $Col_r/p2mm$[e]
THN(9)9	$Col_r/p2mm$ 200 I[d]	I 195[d] $Col_r/p2mm$[e]
THN(9)10	$Col_r/p2mm$ 190 I[d]	I 183[d] $Col_r/p2mm$[e]
THN(9)11	$Col_r/p2mm$ 190 I[d]	I 184[d] $Col_r/p2mm$[e]
THN(9)12	$Col_r/p2mm$ 180 I[d]	I 176[d] $Col_r/p2mm$[e]
THN(9)10B	$Col_r/p2mm$ 154 I[d]	I 142[d] $Col_r/p2mm$[e]

[a]For compounds belonging to **THN(6)n** series, peak temperatures in the DSC traces obtained during the first heating−cooling cycles at 5 °C min^{-1} are given along with the enthalpies (kJ mol^{-1}) of transitions. [b]The temperature of the phase transitions of tris(hydrazone)s belonging to the **THN(9)n** (trialkoxy) series could be determined with the aid of POM only as no events were seen in the DSC traces. [c]This phase (supercools) exists until the limitation (−50 °C) of the DSC instrument; however, the fluidity of the phase decreases in the temperature range of 40−65 °C, but the texture of the Col phase remains unaltered, implying freezing of the phase in the glassy state. [d]The phase transition was observed under POM and too weak to get detected in DSC. [e]This phase (supercools) exists until the limitation (−50 °C) of the DSC instrument. [f]I, isotropic liquid; $Col_h/p6mm$, hexagonal columnar phase with the *p6mm* lattice; $Col_r/p2mm$, columnar rectangular phase with the *p2mm* lattice; Cr, crystal.

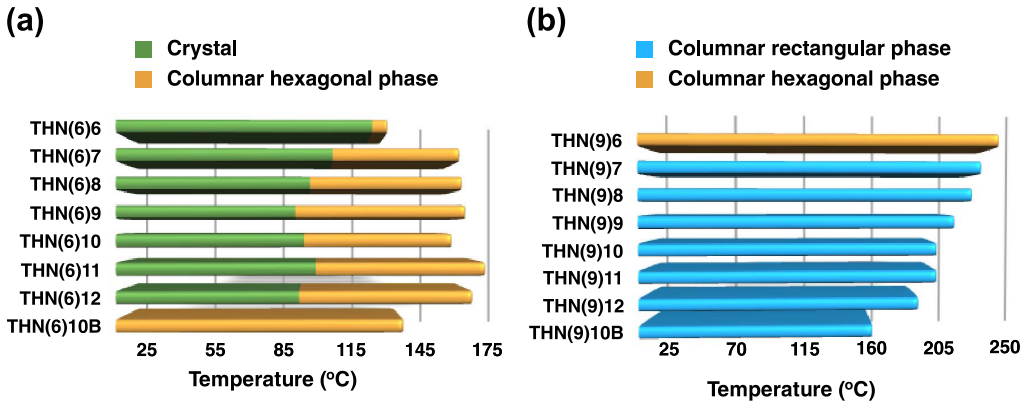

Figure 3. Bar graphs showing the phase transitions/sequences derived from the first heating cycle of discotics of **THN(6)n** (a) and **THN(9)n** (b) series.

the series also exhibited the aforesaid pattern besides other characteristic defect textures of the Col phase such as pseudoisotropic domains, pseudo-focal-conic fan-shaped texture, and dendritic texture (Figure S46). On further cooling, the texture remains unaltered until room temperature (RT). In the DSC trace registered for a cooling run, no exothermic peaks (Figure 4a), except for the signature due to I-Col phase transition, were seen, meaning that the frozen Col phase exists until −50 °C. Moreover, no expected events were detected even when a large amount of samples was used for the calorimetric study. Similar behavior was noted for the next member of the series, namely, **THN(6)7** (Figure S47a). As mentioned earlier, this behavior can be attributed to the slow response of the discogens to the heat or small enthalpy changes, which may be falling well below the recognition limit of DSC equipment.[29] However, DSC curves of the cooling runs of the other members, namely, **THN(6)8**, **THN(6)9**, **THN(6)10**, **THN(6)11**, and **THN(6)12**, comprise two exothermic peaks, implying that these discotics crystallize while cooling from the Col phase (Figure S47b−f). However, the DSC traces of the heating and cooling cycles of **THN(6)10B** (Figure S47g) showed endothermic and exothermic peaks (ΔH = 1.8 kJ mol^{-1}), respectively, confirming that this mesogen is a room-temperature Col LC.

The Col phase formed by discotics **THN(6)6**, **THN(6)8**, **THN(6)10**, and **THN(6)12** was elucidated by the powder XRD technique. The diffraction patterns obtained for the Col phase at the chosen temperatures were obtained while cooling the samples from their isotropic liquid state. The Bragg reflections and other important data/parameters obtained from the XRD profiles are collected in Table 2. For the first sample, **THN(6)6**, the diffraction pattern was collected in the Col phase at 80 °C. The profile shows a characteristic diffuse peak at high angles ($2\theta \sim 20°$, spacing $c \sim 4.4$ Å) that can be

https://dx.doi.org/10.1021/acsomega.0c05779
ACS Omega 2021, 6, 3291−3306

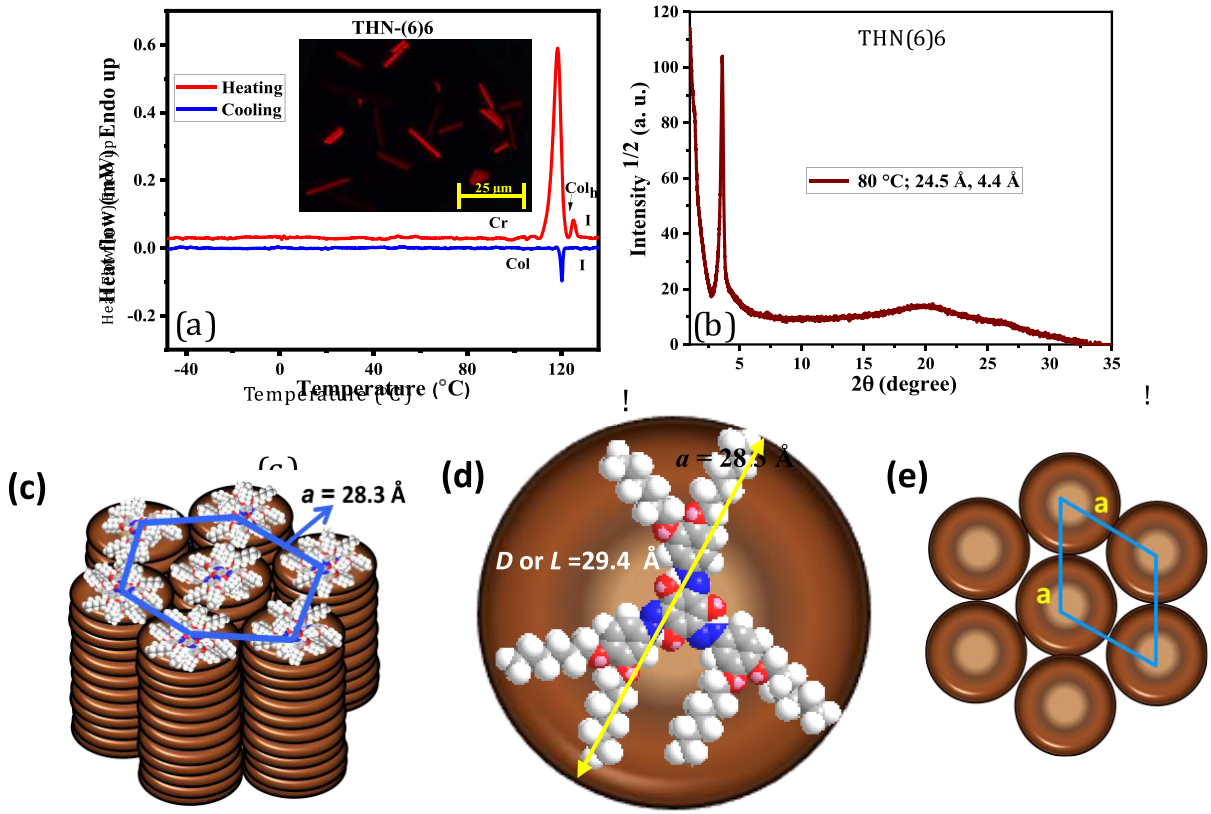

Figure 4. (a) DSC traces obtained for **THN(6)6** during first heating−cooling cycles at a rate of 5 °C min^{-1}; inset: photomicrograph of the texture seen for the Col$_h$ phase of **THN(6)6** at 116 °C. (b) 1D intensity vs 2θ profiles obtained for the Col$_h$/*p6mm* phase of **THN(6)6** at 80 °C. (c) Schematic representation (tilted side-view) of the self-assembly of **THN-(6)6** into the Col$_h$ phase. (d) Space-filling model of **THN-(6)6** in its all-*trans* conformation; *D*, diameter of the disc; *L*, length of the mesogen. (e) Plan view of the 2D lattice in the Col$_h$ phase having a *p6mm* lattice.

ascribed to the liquidlike correlation of the discs within the column and, thus, the fluid nature of the phase is evidenced. The low-angle region ($0 < 2\theta < 5°$) comprises a strong reflection corresponding to a Bragg spacing (d) of 24.5 Å (Figure 4b). In general, the multiple reflections expected for the Col phase are nonexistent; the presence of only one (d_{100}) peak has been generally attributed to a minimum in the form factor that prevents the occurrence of peaks in this angular region. In other words, such a pattern has been assigned to a 2D hexagonal lattice (Col$_h$ phase).[13−18,28] The textural pattern observed also supports the fact that the **THN(6)6** stabilizes the Col$_h$ phase. Thus, the self-assembly via strong $\pi-\pi$ stacking of discogen **THN(6)6** yields columns that eventually pack, along their axes, into the 2D lattice having a hexagonal symmetry (Figure 4c); seemingly, the hexagonal cell parameter "*a*" (28.3 Å) is slightly smaller than that of the diameter of the disc (D)/the length (L) of the mesogen (29.4 Å) (Figure 4d), which can be ascribed to the subtle interdigitation of the peripheral *n*-alkoxy tails (Table 2). The indexing of a Col$_h$ phase, pertaining to the D_{6h} point group symmetry, is relatively simple because of the high symmetry of the *p6mm* plane group, which is equivalent to the *p6/mmm* space group. Thus, the observed Col$_h$ phase in these discogens has been assigned to the *p6mm* symmetry (Figure 4e).

The occurrence of the Col phase in the subsequent (higher) members was also identified based on the observation of the aforementioned textural pattern (Figure S46), which is characteristic of a Col$_h$ phase.[13−15] The structure of the Col phase displayed by **THN(6)8**, **THN(6)10**, and **THN(6)12** was elucidated by the XRD study. To corroborate our inference derived from the POM study that these discotics are monomesomorphic, the X-ray patterns were obtained at different temperatures for the discotics **THN(6)8** and **THN(6)10** as test cases. The 1D intensity vs 2θ profiles obtained for **THN(6)8** (at 80 and 140 °C) and **THN(6)10** (at 100 and 140 °C) have been presented in Figure S48 and b, respectively. The low-angle and wide-angle reflections observed in these profiles are listed in Table 2. As envisaged, the XRD patterns obtained at two different temperatures for the Col phase of discotic **THN(6)8** were found to be qualitatively identical. In the small-angle region of diffractograms, a sharp Bragg (100) peak with the spacings (d) of 26.5 Å (at 80 °C) and 26.1 Å (at 140 °C) was observed. As noted earlier, it is difficult to assign the structure of the Col phase explicitly in the absence of other reflections. However, the presence of one single low-angle maximum is often seen in XRD profiles of the hexagonal Col phase stabilized by different discotics. In addition, in both profiles, a broad and diffuse scattering halo, centered on 4.4 Å, arising from the conformationally disordered aliphatic peripheral chains was observed. Thus, based on textural behavior in conjunction with XRD data, it may be concluded that **THN(6)8** stabilizes the Col$_h$ phase. The POM assessment that the discogens **THN(6)10** and **THN(6)12** show nearly similar Col behavior was evidenced based on the XRD study. Figure S48b,c shows the 1D intensity vs. the 2θ profile for the samples **THN(6)10** and **THN(6)12** at the chosen temperatures. They exhibited indistinguishable XRD patterns with a diffuse and broad-scattering halo seen at wide angles centered around 4.5 Å arising due to the liquidlike order of the alkoxy chains.

https://dx.doi.org/10.1021/acsomega.0c05779
ACS Omega 2021, 6, 3291−3306

Table 2. Data Derived from the Analysis of XRD Profiles Recorded at a Given Temperature (T °C) for the Col Phases Stabilized by Tris(keto-hydrazone) Discogens Belonging to Two Series

entry (D/Å)	phase T/°C symmetry	d/(Å)	lattice parameters (Å) lattice area S (Å^2) molecular volume V (Å^3)	Miller indices (hkl)
THN(6)6 (29.4)	Col_h	24.5	a: 28.3	100
	80		S: 693.1	
	p6mm	4.4	V: 3049.6	
THN(6)8 (33.9)	Col_h	26.5	a: 30.7	100
	80		S: 816.2	
	p6mm	4.4	V: 3591.4	
	Col_h	26.1	a: 30.2	100
			S: 789.9	
	140		V: 3475.4	
	p6mm	4.4		
THN(6)10 (38.7)	Col_h	28.5	a: 32.9	100
	100	16.4	S: 937.4	
	p6mm	4.5	V: 4218.3	
	Col_h	28.1	a: 32.4	100
	140	16.2	S: 909.1	
	p6mm	4.6	V: 4181.9	
THN(6)12 (43.4)	Col_h	29.6	a: 34.2	100
	140	17.1	S: 1012.9	
	p6mm	4.6	V: 4659.5	
THN(9)6 (32.5)	Col_h	23.5	a: 27.1	100
	28	4.3	S: 636.0	
	p6mm		V: 2734.9	
	Col_h	23.5	a: 27.1	100
	40	4.3	S: 636.0	
	P6mm		V: 2734.9	
	Col_h	23.4	a: 27	100
	100	4.3	S: 631.3	
	p6mm		V: 2714.7	
THN(9)9 (40.1)	Col_r	26.2	a: 24.4; b: 26.2	100
	28	24.4	S: 639.3	010
	p2mm	19.6	V: 2812.8	110
		4.4		
	Col_r	26	a: 24; b: 26	100
	60	24	S: 624.0	010
	p2mm	4.6	V: 2870.4	
	Col_r	25.8	a: 25.8	100
	100	27.6	b: 27.6	010
	p2mm	4.6	S: 712.1	
			V: 3275.6	
	Col_r	25.6	a: 23.9; b: 25.6	100
	160	23.9	S: 611.8	010
	p2mm	4.6	V: 2814.5	
	Col_r	25.4	a: 24; b: 25.4	100
	190	24	S: 609.6	010
	p2mm	4.6	V: 2804.2	
THN(9)11 (45.2)	Col_r	29.6	a: 27.6; b: 29.6	100
	28	27.6	S: 816.9	010
	p2mm	4.4	V: 3594.6	
	Col_r	29.5	a: 27.3; b: 29.5	100
	60	27.3	S: 805.4	010
	p2mm	4.6	V: 3704.6	
	Col_r	29.1	a: 27.01; b: 28.08	100
	120	27	S: 758.4	010
	p2mm	4.6	V: 3488.8	
	Col_r	28.6	a: 27.01; b:28.59	100
	170	27	S: 772.2	010

https://dx.doi.org/10.1021/acsomega.0c05779
ACS Omega 2021, 6, 3291−3306

Table 2. continued

entry (D/Å)	phase T/°C symmetry	d/(Å)	lattice parameters (Å) lattice area S (Å^2) molecular volume V (Å^3)	Miller indices (hkl)
	p2mm	4.6	*V*: 3552.2	
THN(9)10B (36.1)	Col_r	29	*a*: 25.15; *b*: 29	100
	50	19	*S*: 729.4	010
	p2mm	12.6	*V*: 3573.8	200
		10.9		210
		4.9		
	Col_r	25.2	*a*: 21.6; *b*: 25.2	100
	130	21.6	*S*: 544.3	010
	p2mm	4.9	*V*: 2667.2	

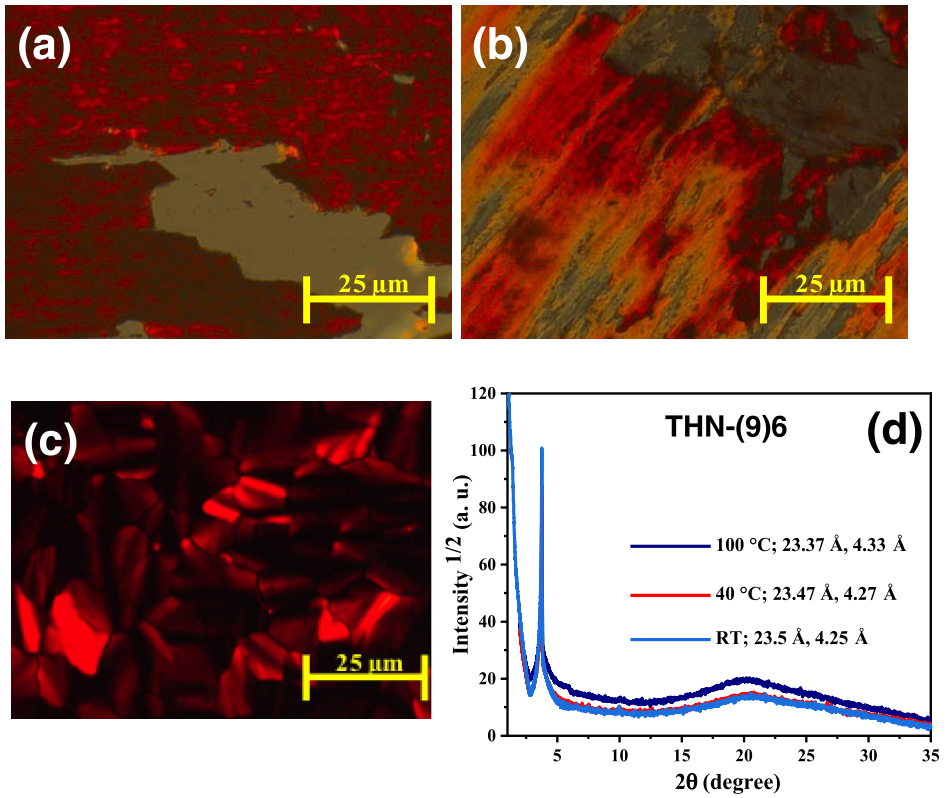

Figure 5. Photomicrographs of the optical textures and XRD profiles of the Col phase of **THN(9)6** discogen. Optical texture of the room-temperature Col phase seen when the sample is placed between glass slides (a) and the top glass plate is pressed down firmly to flatten (b). Texture of the room-temperature Col phase obtained by cooling the isotropic liquid (c). Intensity vs 2θ profiles of the Col_h phase recorded at 100, 40 °C, and at RT (28 °C) (d).

However, in these two materials, the X-ray evidence is less ambiguous in the presence of a second peak at low angles (see Table 2); the ratio of the spacings of the low-angle reflections is 1:0.576, a feature expected of the Col_h phase. Thus, the X-ray data in addition to the defect textures suggest that all of the discotics belonging to **THN(6)n** series self-assemble into the *p6mm* columnar LC structure, meaning that the variation of the length of peripheral flexible chains has no effect on their phase transitional behavior.

Generally, the mesomorphism of discotics can be altered considerably[13] if the central aromatic core is substituted with more numbers of paraffinic chains as they tend to induce additional disorder in the structure. The addition of more flexible chains not only affects the transition temperatures, especially the melting and clearing temperatures, but also changes the mesophase structure. Thus, needless to say, the **THN(9)n** series of tris(keto-hydrazone)s bearing nine alkoxy tails at the periphery behave rather differently from those of the **THN(6)n** series of discotics possessing six alkoxy tails. It is apparent from the data gathered in Table 1 that all eight tris(hydrazone)s show room-temperature columnar phase spanning over a wide thermal range. Specifically, they show the Col phase existing from subambient temperature to well above the RT (28 °C). All of the compounds were found to be viscous, hard (gummy) masses. However, when the samples were sandwiched between microscope glass slides and pressed hard (sheared), they spread out with ease at RT (Figure 5a), and upon withdrawal of the force applied, the flattened mass

https://dx.doi.org/10.1021/acsomega.0c05779
ACS Omega 2021, 6, 3291−3306

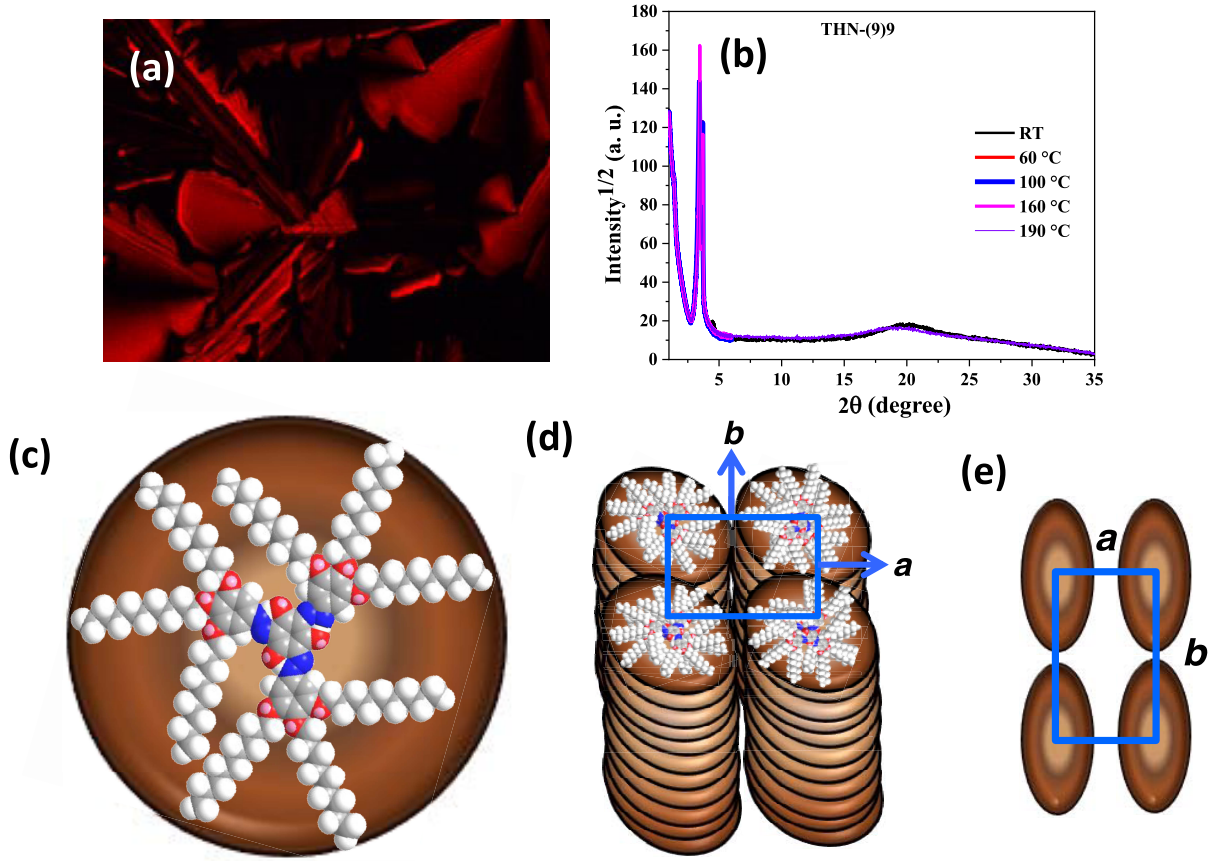

Figure 6. (a) Texture seen at RT for the Col_r phase formed upon cooling from the sample **THN(9)10B** from its isotropic liquid state. (b) 1D intensity vs 2θ profiles obtained for the Col_r phase of **THN(9)9** at five different temperatures, including RT (28 °C). (c) Energy-minimized space-filling model of **THN(9)9**. (d) Schematic representation of the discogens **THN(9)9** self-assembling into the Col_r phase having a *p2mm* lattice (derived from XRD data). (e) Plan view of the 2D lattice of the Col_r phase having a *p2mm* symmetry.

shrinks slowly. Upon sliding the upper glass plate of the sample, a noncharacteristic birefringent texture appears where the dragging marks of samples can be seen (Figure 5b), implying that all of the samples exhibit a highly viscous LC phase at RT (28−30 °C). The first member of the series **THN(9)6** with nine peripheral *n*-hexyloxy chains stabilizes the Col phase that was first established by textural observations. When a thin film of the sample sandwiched between two glass plates is gradually cooled from the isotropic phase, a transition to the Col phase occurs, exhibiting a mosaic textural pattern (Figure 5c), which remains unchanged until RT, where it could be sheared well. The structure of this mesophase was characterized with the aid of the XRD technique. The XRD profiles were collected at three different temperatures, viz., RT, 40, and 100 °C. As expected, all of the diffractograms were found to be practically analogous. The indexed diffraction of 1D intensity vs 2θ profile of the mesophases (Figure 5d) and the results of these studies are collected in Table 2. As can be seen, the diffractograms contain a diffuse scattering halo in the wide-angle region (2$\theta \sim 20°$, spacing $c \sim 4.3$ Å) originating due to the interaction among the floppy alkoxy tails of the columns and suggest that the correlated order is liquidlike. A sharp (single) peak occurring in the low-angle region of the profiles indicates the distance between the adjacent (100) planes (d_{100}) of the Col_h phase. The hexagonal cell parameter "*a*" (~27 Å) derived for each diffractogram that provides the intercolumnar distance was found to be lesser than the fully stretched (all-*trans*) molecular length (32.5 Å) of discogen **THN(9)6** (Table 2), implying that the peripheral chains interdigitate and fill the space between the columns.

The other members of the series, namely, **THN(9)7**, **THN(9)8**, **THN(9)9**, **THN(9)10**, **THN(9)11**, **THN(9)12**, and **THN(9)10B**, show different optical textural patterns when compared to that of **THN(9)6** (Figure S46). For example, the Col phase formed upon cooling from the isotropic liquid of compound **THN(9)10B** displays a striking pseudo-leaf-like (fern-like) texture with intermixed bright and dark areas as shown in Figure 6a. As representative cases, the structure of the Col phase formed by **THN(9)6**, **THN-(9)9**, **THN(9)11**, and **THN(9)10B** was subjected to XRD studies. The diffractograms for the compound **THN(9)9** were obtained at five different temperatures: RT (28 °C), 60, 100, 160, and 190 °C (Figure 6b and Table 2). The diffractograms obtained at RT show, apart from a diffuse and broad-scattering halo at wide angles centered around 4.4 Å, three sharp reflections in the small-angle with spacings of (*d*) 26.2, 24.4, and 19.6, which could be indexed to the 2D-rectangular lattice. As is known, in the Col_r phase, the disk planes are perpendicular to the column axis; that is, disklike mesogens **THN(9)9** (Figure 6c) tilt with respect to the column axis, and hence, the individual columns or cross sections of the columns appear elliptical when viewed from the top of the 2D lattice structure (Figure 6d). Four different symmetries, such as *p2mm*, *c2mm*, *p2gg*, and *p2mg*, have been assigned to rectangular 2D lattices; the latter three symmetries belong to planar space groups *C2/m*, *P21/a*, and *P2/a*, respectively. However, the aforesaid three low-angle

https://dx.doi.org/10.1021/acsomega.0c05779
ACS Omega 2021, 6, 3291−3306

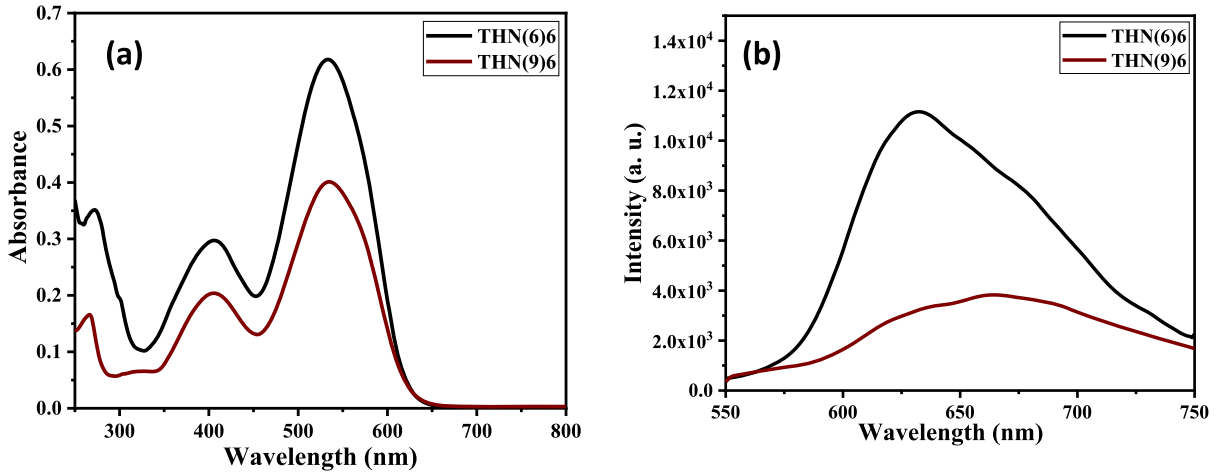

Figure 7. UV−vis (a) and (b) emission spectra of discotic LCs **THN(6)6** and **THN(9)6** in the micromolar dichloromethane (DCM) solution.

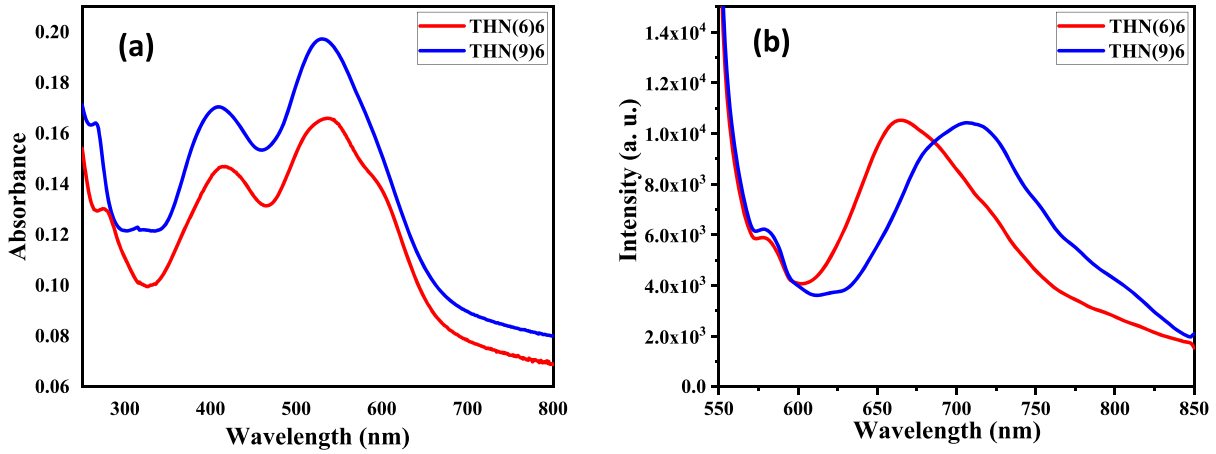

Figure 8. Solid-state (thin-film) absorption (a) and emission (b) spectra of **THN(6)6** and **THN(9)6**.

peaks could be indexed to the (01), (10), and (02) planes of a rectangular 2D structure having a *p2mm* lattice with the parameters a = 26.2 Å and b = 24.4 Å (Figure 6d and Table 2). Plan view of the 2D lattice of the Col_r phase having a *p2mm* symmetry is illustrated in Figure 6e. As shown in Tables 1 and 2, based on the indexation of the XRD patterns, it was possible to assign a *p2mm* symmetry to the rectangular 2D lattice of the Col_r phase formed for other members of the **THN(9)n** series of compounds. Seemingly, the XRD profiles obtained at above temperatures for **THN(9)9** were found to be qualitatively identical to those of the diffractograms recorded for the tris(hydrazone)s **THN(9)11** (Figure S48d) and **THN(9)10B** (Figure S48e) at different temperatures with an exception that the profile of the latter compound obtained close to room temperature (50 °C) shows four sharp reflections in the low-angle region, which could be indexed to fit into a 2D-rectangular lattice. In the small-angle region, all of the patterns show two sharp reflections, which follow a reciprocal spacing ratio of 1:0.8−0.93; these are indexed as (100) and (010), reflections from a 2D-rectangular lattice with cell parameters a = 21.6−27.6 Å and b = 25.2−29.6 Å. Hence, the X-ray data (Table 2) along with the textural patterns (Figure 6a) confirm that the mesophase is indeed the Col_r phase. Thus, compounds **THN(9)7**, **THN(9)8**, **THN(9)9**, **THN(9)10**, **THN(9)11**, **THN(9)12**, and **THN(9)10B** stabilize the columnar rectangular phase with the *p2mm* lattice, while the first member **THN(9)6** stabilizes the columnar hexagonal phase featuring the *p6mm* lattice.

Photophysical Studies. Given the fact that these C_3-symmetric, [n,π]-conjugated functional molecules, the tris-(keto-hydrazone)s, show interesting optical properties, we expected the discotics realized in the present study to exhibit photophysical (UV−vis absorption and fluorescence) characteristics. In particular, the UV−vis absorption and fluorescence characteristics of the compounds were studied in their solutions (Figures 7 and S49), as well as in condensed (solid) (Figures 8 and S50) and mesomorphic states (Figures S10 and S51) The photophysical properties derived from these studies are collected in Table 3. For example, we explain the studies on the micromolar solution (in CH_2Cl_2) and the thin film of compounds **THN(6)6** and **THN(9)6**. Like TSANs, this compound **THN(6)6** exhibited two absorption maxima centered around 407 and 534 nm corresponding to $\pi-\pi^*$ and $n-\pi^*$ transitions, respectively (Figure 7a, black trace). On excitation in the solution state, at their absorption maxima (λ_{max} = 534 nm), a dark-red emission was observed (λ_{max} = 632 nm, Figure 7b, black trace); this is noteworthy because the red-light-emitting compounds are very scarce, and they provide a doorway to fine-tune the emission on combining with another dopant emitter.

The absorption spectrum of **THN(9)6** was similar to that of **THN(6)6**, while a slight red shift was noticed in the emission

https://dx.doi.org/10.1021/acsomega.0c05779
ACS Omega 2021, 6, 3291−3306

Table 3. Photophysical Properties of THN(6)n and THN(9)n Series of Discotic LCs

	DCM solution[a]			solid state (drop-cast thin film)		
discotics	absorption[b]	emission[b,c]	Stokes shift	absorption[b]	emission[b,c]	Stokes shift
THN(6)6	272, 407, 532	633	101	275, 417, 537	584, 665	128
THN(6)7	274, 412, 540	646	106	276, 417, 535	584, 676	141
THN(6)8	274, 413, 539	648	109	275, 417, 538	589, 674	136
THN(6)9	274, 414, 539	644	105	276, 415, 525	576, 670	145
THN(6)10	274, 414, 539	641	102	281, 423, 545	597, 667	122
THN(6)11	274, 413, 540	644	104	280, 423, 549	594, 673	124
THN(6)12	274, 414, 539	645	106	279, 423, 545	594, 672	127
				Col LC state (thin film)		
				absorption[b]	emission[b,c]	Stokes shift
THN(9)6	266, 405, 535	664	129	266, 409, 530	583, 706	176
THN(9)7	266, 406, 535	670	135	266, 411, 527	581, 680	153
THN(9)8	266, 406, 535	673	138	266, 409, 534	581, 686	152
THN(9)9	275, 413, 541	649	108	273, 424, 545	580, 699	154
THN(9)10	266, 406, 535	668	133	266, 410, 531	580, 685	154
THN(9)11	266, 405, 535	656	121	270, 410, 538	581, 669	131
THN(9)12	266, 405, 535	655	120	266, 408, 539	581, 692	153

[a]Micromolar solutions in DCM. [b]Wavelengths (nm). [c]Excitation wavelength = 535 nm.

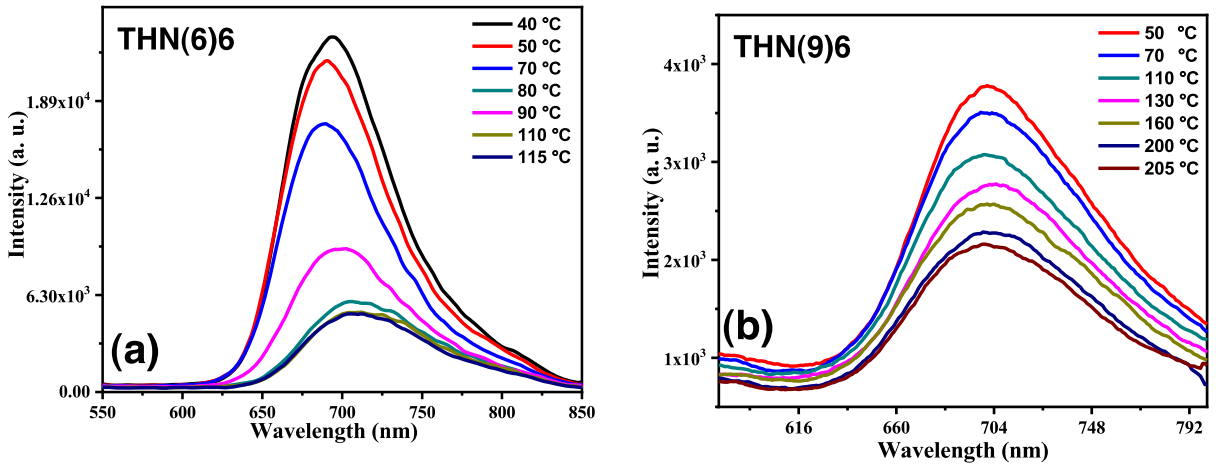

Figure 9. Emission spectra recorded as a function of temperature for the Col phases of **TNH(6)6** (a) and **TNH(9)6** (b).

band (Figure 7a,b, brown trace). In general, a Stokes shift of 100−140 nm was observed, which makes it easier to discriminate the emitted light and excitation light. It further reduces the probability of reabsorption of the emitted light (which leads to emission quenching). Relative quantum yields of compounds **THN(6)6** and **THN(9)6** were measured with respect to Rhodamine-B solution and were found to be 4.5 and 9.8%, respectively (Table S1 and Figure S52). Furthermore, using the UV−vis absorption data of the micromolar DCM solutions (Table 3), the energy band gap of these discotics was studied. The optical band-gap values were determined from the longest wavelength absorption onset of the UV−vis spectra of mesogens using the expression $E = 1240/\lambda_{onset}$. The results revealed that these materials exhibit band gap in the range of 1.8−1.9 eV, which is low.

The general tendency of fluorescent LCs to aggregate in condensed phases like solids, mesophases, and liquids often leads to detrimental aggregation-caused quenching (ACQ)[30−32] due to the intermolecular energy transfer.[33] Thus, one has to overcome the ACQ problem by some strategy to realize novel solid/LC fluorescent materials. Therefore, absorption and fluorescence properties of all of the **THN(6)n** and **THN(9)n** series of compounds were investigated. The thin films of these compounds were prepared by drop-casting the solutions on the quartz substrate. The absorption and fluorescence spectra recorded at room temperature for these thin films are provided in Figures 8 and S50. As an example, an overlay of absorption and emission spectra of representative compounds **THN(6)6** and **THN(9)6** in a thin-film state is provided in Figure 8. The absorption spectra were broad compared to their solution-state spectra; however, the absorption maxima did not differ much. In contrast, the emission spectra exhibited a significant red shift of almost 30−40 nm (Table 3). In other words, the solution-state emission maxima were centered around 630−673 nm, while in the solid state, the emission maxima were centered around 660−710 nm.

The emission behavior of the fluid Col phase in the thin-film state was also investigated with respect to temperature variation. The sample under investigation was placed between the two glass coverslips and cooled slowly (1 °C min^{-1}) from the isotropic state until RT. The wavelength λ_{ex} = 534 nm was used for the excitation. At first, the fluorescence spectra were recorded at lower temperatures, and subsequently, the sample

https://dx.doi.org/10.1021/acsomega.0c05779
ACS Omega 2021, 6, 3291−3306

was heated to the required temperatures where the emission spectra were recorded. As can be seen in Figure 9, the emission intensity drops progressively with the rise in temperature, which can be accredited to the collapse of larger columnar stacks into smaller ones and thermally activated radiationless processes.[13−17] A similar trend was noted for other discotics also (Figure S51).

Remarkably, in comparison with the solution-state emission, the films of the neat Col phase show a substantial bathochromic (red) shift, which can be accredited to the strong cofacial proximity of C_{3h} cores within the Col structure in addition to the formation of excimers/aggregates.[26] Therefore, the tris(hydrazone)s realized in this work are capable of emission in both solution and mesophase states. Nonetheless, detailed investigations are necessary concerning the annealing of films, film morphology, fluorescence efficiency, solvent effects, etc., to interpret further the photophysical properties of tris(keto-hydrazone)s quantitatively.

CONCLUSIONS

A new class of discotic liquid crystals based on tris(hydrazone)s existing only in the C_{3h} isomeric keto-enamine form has been designed and synthesized. A systematic study was undertaken to determine the structure−property correlation. Tris(hydrazone)s with six (**THN(6)n** series) and nine (**THN(9)n** series) peripheral *n*-alkoxy/branched tails (in the form of three 1,2-bis(alkoxy)benzenes or 1,2,3-tris(alkoxy)-benzenes) displayed columnar behavior. X-ray data supported by the POM observations suggested that the **THN(6)n** series of compounds stabilized the Col_h phase. This clearly suggests that the variation of the peripheral chain length has no effect on the phase transitional behavior of **THN(6)n** series of compounds. Likewise, the X-ray data in conjunction with the textural patterns seen propose that the mesophase stabilized by the **THN(9)n** series of compounds is indeed the Col_r phase with the exception of the first member of the series that exhibits the Col_h phase. Most importantly, **THN(9)n** series of tris(hydrazone)s shows the Col phase existing from sub-ambient temperature to well above the ambient temperature. The studies on photophysical properties enabled demonstrating the light-emitting capabilities of these discotic tris(hydrazone)s in both solution and mesophase states. This can be ascribed to the extended π-conjugations among the arms and the central core. As expected, irrespective of the variations in the number and length of the peripheral alkoxy tails, they exhibit almost identical photophysical features. The observed light-emissive characteristics of these systems are promising for application in organic electronics considering the fact that in such structures, the proton and electron interact with each other through the H-bonding environment. In particular, the occurrence of the intense emissive band in the low-temperature Col phase, that too in the deep-red/NIR region, is noteworthy as such properties are much sought-after for the bioimaging as well as for the construction of OLEDs. From the absorption spectra, it was found that these compounds exhibit a low energy gap (1.82−1.89 eV). In a nutshell, due to the ease of synthesis, structural diversity, columnar behavior, and electronic properties, this new class of discotic tris(hydrazone)s may find increased interest in the design of new materials for organic electronic devices.

EXPERIMENTAL SECTION

General Remarks. *Chemicals and Solvents.* The requisite chemicals/reagents and analytical-grade solvents were procured from overseas as well as local companies. Bulk solvents used for purification/extraction and other general purposes were purchased from local sources. Unless otherwise specified, chemicals/reagents were used as received from the suppliers without further purification. The bulk solvents were purified prior to use by following standard distillation methods.

Monitoring and Purification. Thin-layer chromatography (TLC) was used not only to monitor the progress and completion of reactions but also to evaluate the purity of the materials. TLC plates derived from aluminum sheets precoated with silica gel (Merck, Kieselgel60, F254) were used. Silica gels of mesh sizes 60−120, 100−200, and 230−400 were used as stationary phases in column chromatography purification.

Molecular Structural Characterization. In general, the target liquid crystalline materials and their intermediates were characterized structurally with the aid of UV−vis, FTIR, and NMR spectroscopic techniques. Electronic absorption (UV−vis) spectroscopy was performed using a PerkinElmer Lambda 20 UV−vis spectrometer. IR spectra were recorded with a PerkinElmer Spectrum 1000 FTIR spectrometer; the spectral positions are given in wavenumbers (cm^{-1}). Proton (^1H) and carbon (^{13}C) NMR spectra were recorded in $CDCl_3$ with a Bruker AMX-400 (400 MHz) spectrometer at ambient temperature; the chemical shifts (δ) are reported in parts per million (ppm) relative to the chemical shift of tetramethylsilane (TMS) as an internal standard; coupling constants (J) are given in Hz. Mass spectra of the compounds were recorded with a JEOL JMS-600H spectrometer (Tokyo, Japan) in the FAB+ mode using 3-nitrobenzyl alcohol as a liquid matrix. Mass spectra were determined on a JEOL JMS-600H spectrometer in the FAB+ mode using 3-nitrobenzyl alcohol as a liquid matrix. Elemental microanalysis data of the final compounds were obtained with a PerkinElmer 2400 Series II CHNS/O elemental analyzer.

Mesomorphic and Photophysical Studies. The liquid crystal properties of the mesogens were revealed with the aid of an Olympus BX50, model BX50F4 optical polarizing microscope, attached to a digital camera and a Mettler FP82HT hot-stage programmed by an FP90 Central Processor, and a PerkinElmer Diamond differential scanning calorimeter (DSC) with a PC system operating Pyris software. The DSC instrument prior to sample measurement was calibrated using pure indium as a standard. DSC traces recorded at a scanning rate of 58 °C min^{-1} were employed to determine the transition temperatures and associated enthalpies. X-ray diffraction (XRD) studies with Cu Kα/(λ = 0.15418 nm) radiation were carried out using a powder X-ray diffractometer, namely, PANalytical X'Pert, PRO MP machine, consisting of a focusing elliptical mirror and a fast resolution detector (PIXCEL). The samples under XRD investigation were filled in Lindemann capillaries (0.5 mm diameter) in their isotropic state by capillary action, and both ends of the capillaries were flame-sealed carefully. The compounds' molecular length was calculated from the energy-minimized structure deduced from the CS Chem 3D version 9 program. Fluorescence emission spectra were recorded using a Fluorolog spectrofluorometer (HORIBA JOBIN YVON) in conjunction with a programmable hot stage (INSTEC HCS 402). The relative quantum yield technique was used for the determi-

https://dx.doi.org/10.1021/acsomega.0c05779
ACS Omega 2021, 6, 3291−3306

nation of quantum yield. Rhodamine-B dissolved in water was used as an internal standard.

*Synthesis and Characterization. 1,2-Bis(nonyloxy)-benzene (**1d**).* A mixture of catechol (5 g, 45.40 mmol, 1 equiv), anhyd. K_2CO_3 (181.63 mmol, 4 equiv), catalytic amount of potassium iodide, *n*-bromononane (99.9 mmol, 2.2 equiv), and dry DMF (30 mL) was stirred at 80 °C for 12 h under a dry nitrogen atmosphere. The reaction mixture was then poured into cold water (300 mL), and the crude product was extracted with dichloromethane (3 × 100 mL). The combined extracts were washed with water (300 mL) followed by brine, dried over anhyd. Na_2SO_4, and concentrated. The crude product was purified by column chromatography using neutral alumina. The column was initially eluted with hexanes to remove the unreacted *n*-bromononane followed by 5% EtOAc-hexanes to yield the pure product. R_f = 0.54 in 50% CH_2Cl_2-hexanes; a colorless liquid; yield: 14 g (85%); IR (neat): ν_{max} in cm^{-1} 2931, 2858, 1593, 1503, 1255, 1224, 1124, and 739; ^1H NMR ($CDCl_3$, 400 MHz): δ 6.88 (s, 4H, Ar), 4.00 (t, 4H, J = 8 Hz, 2 × OCH_2), 1.87−1.28 (m, 28H, 14 × CH_2), 0.89 (t, 6H, J = 8 Hz, 2 × CH_3); MS (FAB^+): m/z calcd for $C_{24}H_{42}O_2$: 362.3; found: 362.2. Anal. calcd for $C_{24}H_{42}O_2$: C, 79.50; H, 11.68; found: C, 79.42; H, 11.65.

*1-Nitro-3,4-bis(nonyloxy)benzene (**2d**).* To a clear solution of 1,2-bis(nonyloxy)benzene (17.96 mmol, 1 equiv) in dry CH_2Cl_2 (30 mL), a catalytic amount of $NaNO_2$ (2.5 mmol, 0.14 equiv) was added. The reaction mixture was cooled to −10 °C, and fuming HNO_3 (1.1 mL, 13.2 mmol, 1 equiv) was added dropwise while maintaining the temperature below −5 °C for 15 min. The completion of the reaction was indicated by a drastic change in the color from greenish blue to pale yellow, which was further confirmed by TLC. The reaction mixture was washed with water (3 × 100 mL) and brine (50 mL), dried over anhyd. Na_2SO_4, and concentrated to yield a pale-yellow solid, which was purified by recrystallization from EtOH. R_f = 0.50 in 30% CH_2Cl_2-hexanes; pale-yellow solid; yield: 3.20 g (57%); mp: 64−65 °C; IR (KBr pellet): ν_{max} in cm^{-1} 2953, 2916, 2847, 1590, 1511, 1468, 1347, 1213, 1024, 850, 720; ^1H NMR (400 MHz, $CDCl_3$): δ 7.88 (dd, J_1 = 8.8 Hz, J_2 = 2.4 Hz, 1H, Ar), 7.73 (d, J = 2.4 Hz, 1H, Ar), 6.88 (d, J = 8.8 Hz, 1H, Ar), 4.08 (m, 4H, 2 × OCH_2), 1.87−1.29 (m, 28H, 14 × CH_2), 0.90 (t, J = 6.4 Hz, 6H, 2 × CH_3); MS (FAB +): m/z calcd for $C_{24}H_{42}NO_4$ (M + 1): 408.3; found: 408.4. Anal. calcd for $C_{24}H_{41}NO_4$: C, 70.72; H, 10.14; N, 3.44; found: C, 70.68; H, 10.15; N, 3.28.

*1-Amino-3,4-bis(nonyloxy)benzene (**3d**).* 4-Nitro-1,2-bis-(nonyloxy)benzene (4.6 mmol, 1 equiv) was dissolved in dry THF (30 mL), and 10% Pd-C (10% weight of the starting material) was added. The reaction mixture was degassed and stirred under H_2 gas (1 atmospheric pressure) for 12 h at rt. The reaction mixture was filtered over a Celite bed and concentrated, and the solid obtained was purified by column chromatography using neutral alumina. The column was initially eluted with hexanes and then with 10% EtOAc-hexanes to get the pure product. R_f = 0.43 in 30% EtOAc-hexanes; a viscous liquid; yield: 0.82 g (88%); IR (neat): ν_{max} in cm^{-1} 3347, 2923, 2854, 1514, 1469, 1274, 1230, 1183, 833, 722; ^1H NMR (400 MHz, $CDCl_3$): δ 6.74 (d, J = 8.4 Hz, 1H, Ar), 6.34 (d, J = 2.4 Hz, 1H, Ar), 6.26 (dd, J_1 = 8.0 Hz, J_2 = 3.2 Hz, 1H, Ar), 3.95 (m, 4H, 2 × OCH_2), 3.11 (brs, 2H, NH_2), 1.81−1.30 (m, 28H, 14 × CH_2), 0.90 (t, J = 6.8 Hz, 6H, 2 × CH_3); MS (FAB+): m/z calcd for $C_{24}H_{44}NO_2$ (M + 1): 378.3; found: 378.0. Anal. calcd for $C_{24}H_{43}NO_2$: C, 76.34; H, 11.48; N, 3.71; found: 76.23; H, 11.55; N, 3.59.

*1,2,3-Tris(nonyloxy)benzene (**4d**).* 1,2,3-Trihydroxy benzene (5 g, 39.7 mmol, 1 equiv) was dissolved in a minimum quantity of dry DMF (15 mL), and anhyd. K_2CO_3 (238.1 mmol, 6 equiv) and a catalytic amount of potassium iodide (pinch) were added. To the above suspension, 1-bromononane (130.9 mmol, 3.3 equiv) was added and stirred at 80 °C for 12 h under a dry nitrogen atmosphere. The cooled reaction mixture was poured into cold water (500 mL), and the crude product was extracted with dichloromethane (4 × 100 mL). The combined extracts were washed with water (300 mL) followed by brine, dried over anhyd. Na_2SO_4, and concentrated. The crude product was purified by column chromatography using neutral alumina. The column was initially eluted with hexanes to remove the unreacted 1-bromononane and then with 5% EtOAc-hexanes to get the pure product. R_f = 0.57 in 50% CH_2Cl_2-hexanes; a colorless liquid; yield: 11.01 g (55%); IR (neat): ν_{max} in cm^{-1} 2924, 2854, 1596, 1494, 1299, 1252, 1006, 773, 723; ^1H NMR (400 MHz, $CDCl_3$): δ 6.92 (t, J = 8.4 Hz, 1H, Ar), 6.55 (d, J = 8.4 Hz, 2H, Ar), 3.98−3.93 (m, 6H, 3 × OCH_2), 1.83−1.28 (m, 42H, 21 × CH_2), 0.90 (t, J = 6.4 Hz, 9H, 3 × CH_3); MS (FAB+): m/z calcd for $C_{33}H_{61}O_3$ (M + 1): 505.5; found: 505.4. Anal. calcd for $C_{33}H_{60}NO_3$: C, 78.51; H, 11.98; found: 78.45; H, 11.85.

*5-Nitro-1,2,3-tris(nonyloxy)benzene (**5d**).* To a clear solution of 1,2,3-tris(nonyloxy)benzene (13.2 mmol, 1 equiv) in dry CH_2Cl_2 (25 mL), a catalytic amount of $NaNO_2$ (1.8 mmol, 0.14 equiv) was added, and the reaction mixture was cooled to −10 °C. Fuming HNO_3 (0.8 mL, 13.2 mmol, 1 equiv) was added dropwise while maintaining the temperature below −5 °C. A drastic change in the color of the reaction mixture from greenish blue to pale yellow indicated the completion of the reaction, which was further confirmed by TLC. The reaction mixture was washed with water (3 × 100 mL) and brine (50 mL), dried over anhyd. Na_2SO_4, and concentrated to yield the crude product, which was further purified by column chromatography on silica gel (60−120 mesh). Initial eluting with the hexanes followed by 20% dichloromethane-hexanes yielded the desired product, which was further purified by recrystallization from ethanol. R_f = 0.52 in 30% CH_2Cl_2-hexanes; yellow liquid; yield: 3.10 g, 57%; IR (neat): ν_{max} in cm^{-1} 2916, 2847, 1511, 1347, 1212, 1123; ^1H NMR (400 MHz, $CDCl_3$): δ 7.47 (s, 2H, Ar), 4.07 (m, 6H, 3 × OCH_2), 1.87−1.29 (m, 42H, 21 × CH_2), 0.90 (t, 9H, J = 6 Hz, 3 × CH_3); MS (FAB+): m/z calcd for $C_{33}H_{60}NO_5$(M + 1): 550.83; found: 551.1. Anal. calcd for $C_{33}H_{59}NO_5$: C, 72.09; H, 10.82; N, 2.55; found: 71.98; H, 10.75; N, 2.54.

*1-Amino-3,4,5-tris(nonyloxy)benzene (**6d**).* 1-Nitro-3,4,5-tris(nonyloxy)benzene (2.36 mmol, 1 equiv) was dissolved in dry THF, and 10% Pd-C (10% weight of the nitro compound) was added. The reaction mixture was degassed and stirred under H_2 gas (1 atmospheric pressure) for 12 h at rt. The reaction mixture was filtered over a Celite bed and concentrated. The crude was purified over a neutral alumina column using hexanes followed by 10% EtOAc-hexanes to obtain the pure compound. R_f = 0.43 in 30% EtOAc-hexanes; an off-white solid; mp: 70−71 °C; yield: 0.85 g, 90%; IR (KBr pellet): ν_{max} in cm^{-1} 3417, 2921, 2854, 1632, 1231, 1111, 1026; ^1H NMR (400 MHz, $CDCl_3$): δ 6.27 (s, 2H, Ar), 3.97 (m, 6H, 3 × OCH_2), 1.80−1.27 (m, 42H, 21 × CH_2), 0.89 (t, J = 6.8 Hz, 9H, 3 × CH_3); MS (FAB^+): m/z calcd for

https://dx.doi.org/10.1021/acsomega.0c05779
ACS Omega 2021, 6, 3291−3306

$C_{33}H_{61}NO_3$: 519.5; found: 519.4. Anal. calcd for $C_{33}H_{61}NO_3$: C, 76.24; H, 11.83; N, 2.69; found: 76.18; H, 11.81; N, 2.71.

*Synthesis and Characterization of Tris(keto-hydrazone)s: **THN(6)n and THN(9)n**.* Alkoxy aniline (**3a**−**h**)/(**6a**−**h**) (0.51 mmol, 1 equiv) was dissolved in THF/methanol (1:1). To this solution was added 3 mL of 2 M HCl. The solution was cooled to −5 °C, and $NaNO_2$ (0.07 g, 1.02 mmol, 2 equiv) solution was added dropwise. The reaction mixture was warmed to rt, and a solution of phloroglucinol (0.02 g, 0.153 mmol, 3 equiv) in methanol/2 M NaOH was added dropwise. The reaction mixture was stirred for 30 min. The pH of the reaction mixture was made to neutral, the mixture was diluted with water, and the crude product was extracted with dichloromethane (3 × 30 mL). The crude product was column-chromatographed with neutral alumina as a stationary phase. Initial elution with hexanes followed by 20% EtOAc-hexanes resulted in the desired compound. This was further purified by recrystallization using ethanol.

*2,4,6-Tris(2-(4-bis(3,4-hexyloxy)phenyl)hydrazono)-cyclohexane-1,3,5-trione (**THN(6)6**).* A wine-red solid; yield: 0.095 g, 60%; IR (KBr pellet): ν_{max} in cm^{-1} 3428, 2927, 2857, 1588, 1480, 1268, 1161, 1058, 848; UV−vis: λ_{max} = 541.0 nm, $\varepsilon = 3.11 \times 10^3$ L mol^{-1} cm^{-1}; ^{1}H NMR (400 MHz, $CDCl_3$): δ 16.62 (s, 3H, 3 × NH), 7.26 (s, 3H, Ar), 7.10 (dd, J_1 = 8.8 Hz, J_2 = 2.4 Hz, 3H, Ar), 6.91 (d, J = 8.4 Hz, 3H, Ar), 4.10 (m, 12H, 6 × OCH_2), 2.17−0.92 (m, 66H, 24 × CH_2, 6 × CH_3); ^{13}C NMR (100 MHz): 178.3, 150.5, 149.2, 135.2, 128.2, 113.8, 110.8, 102.7, 69.6, 69.5, 53.4, 31.6, 30.9, 2 9.2, 28.7, 22.6, 14.0. Anal. calcd for $C_{60}H_{90}N_6O_9$: C, 69.33; H, 8.73; N, 8.09; found: C, 69.18; H, 8.55; N, 7.98.

*2,4,6-Tris(2-(4-bis(3,4-heptyloxy)phenyl)hydrazono)-cyclohexane-1,3,5-trione (**THN(6)7**).* A wine-red solid; yield: 0.100 g (58%); IR (KBr pellet): ν_{max} in cm^{-1} 3446, 2926, 2856, 1587, 1470, 1268, 1130, 1058, 848; UV−vis: λ_{max} = 541.6 nm, $\varepsilon = 6.78 \times 10^3$ L mol^{-1} cm^{-1}; ^{1}H NMR (400 MHz, $CDCl_3$): δ 16.62 (s, 3H, 3 × NH), 7.25 (s, 3H, Ar), 7.10 (dd, J_1 = 8.8 Hz, J_2 = 2.4 Hz, 3H, Ar), 6.91 (d, J = 8.8 Hz, 3H, Ar), 4.10 (m, 12H, 6 × OCH_2), 1.88−0.92 (m, 78H, 30 × CH_2, 6 × CH_3); ^{13}C NMR (100 MHz): 178.3, 150.5, 149.1, 135.2, 128.2, 113.8, 110.7, 102.7, 69.6, 69.4, 31.8, 29.3, 29.2, 29.1, 26.0, 25.9, 22.6, 14.1. Anal. calcd for $C_{66}H_{102}N_6O_9$: C, 70.55; H, 9.15; N, 7.48; found: C, 70.75; H, 9.07; N, 7.39.

*2,4,6-Tris(2-(4-bis(3,4-octyloxy)phenyl)hydrazono)-cyclohexane-1,3,5-trione (**THN(6)8**).* A wine-red solid; yield: 0.098 g, 53%; IR (KBr pellet): ν_{max} in cm^{-1} 3428, 2927, 2857, 1588, 1481, 1268, 1129, 1058, 848; UV−vis: λ_{max} = 541.7 nm, $\varepsilon = 4.71 \times 10^3$ L mol^{-1} cm^{-1}; ^{1}H NMR (400 MHz, $CDCl_3$): δ 16.63 (s, 3H, 3 × NH), 7.26 (s, 3H, Ar), 7.11 (dd, J_1 = 8.4 Hz, J_2 = 2.4 Hz, 3H, Ar), 6.91 (d, J = 8.8 Hz, 3H, Ar), 4.10 (m, 12H, 6 × OCH_2), 1.87−0.88 (m, 90H, 36 × CH_2, 6 × CH_3); ^{13}C NMR (100 MHz): 178.3, 150.5, 149.2, 135.2, 128.2, 113.8, 110.8, 102.7, 69.6, 69.5, 31.8, 29.4, 29.3, 29.2, 26.0, 22.7, 14.1. Anal. calcd for $C_{72}H_{114}N_6O_9$: C, 71.60; H, 9.51; N, 6.96; found: C, 71.55; H, 9.55; N, 6.82.

*2,4,6-Tris(2-(4-bis(3,4-nonyloxy)phenyl)hydrazono)-cyclohexane-1,3,5-trione (**THN(6)9**).* A wine-red solid; yield: 0.115 g, 58%; IR (KBr pellet): ν_{max} in cm^{-1} 3428, 2927, 2857, 1589, 1477, 1229, 1058, 848; UV−vis: λ_{max} = 539.1 nm, $\varepsilon = 7.42 \times 10^3$ L mol^{-1} cm^{-1}; ^{1}H NMR (400 MHz, $CDCl_3$): δ 16.63 (s, 3H, 3 × NH), 7.26 (s, 3H, Ar), 7.10 (dd, J_1 = 8.8 Hz, J_2 = 2.4 Hz, 3H, Ar), 6.91 (d, J= 8.8 Hz, 3H, Ar), 4.10 (m, 12H, 6 × OCH_2), 1.85−0.87 (m, 102H, 42 × CH_2, 6 × CH_3); ^{13}C NMR (100 MHz): 178.3, 150.5, 149.1, 113.8, 110.7, 102.7, 69.6, 69.4, 31.9, 29.6, 29.4, 29.3, 26.0, 22.7, 14.1. Anal. calcd for $C_{78}H_{126}N_6O_9$: C, 72.52; H, 9.83; N, 6.51; found: C, 72.44; H, 9.96; N, 6.65.

*2,4,6-Tris(2-(4-bis(3,4-decyloxy)phenyl)hydrazono)-cyclohexane-1,3,5-trione (**THN(6)10**).* A wine-red solid; yield: 0.109 g, 52%; IR (KBr pellet): ν_{max} in cm^{-1} 3474, 2925, 2855, 1589, 1449, 1230, 1065, 827; UV−vis: λ_{max} = 540.7 nm, $\varepsilon = 4.52 \times 10^3$ L mol^{-1} cm^{-1}; ^{1}H NMR (400 MHz, $CDCl_3$): δ 16.63 (s, 3H, 3 × NH), 7.26 (s, 3H, Ar), 7.10 (dd, J_1 = 8.8 Hz, J_2 = 2 Hz, 3H, Ar), 6.91 (d, J = 8.4 Hz, 3H, Ar), 4.10 (m, 12H, 6 × OCH_2), 1.87−0.87 (m, 114H, 48 × CH_2, 6 × CH_3); ^{13}C NMR (100 MHz): 178.3, 150.5, 149.2, 135.2, 128.2, 113.9, 110.7, 102.7, 31.9, 29.6, 29.4, 29.3, 29.2, 14.1. Anal. calcd for $C_{84}H_{138}N_6O_9$: C, 73.32; H, 10.11; N, 6.11; found: C, 73.20; H, 10.23; N, 6.15.

*2,4,6-Tris(2-(4-bis(3,4-undecyloxy)phenyl)hydrazono)-cyclohexane-1,3,5-trione (**THN(6)11**).* A wine-red solid; yield: 0.121 g, 54%; IR (KBr pellet): ν_{max} in cm^{-1} 3475, 2925, 2856, 1589, 1449, 1230, 1123, 827; UV−vis: λ_{max} = 540.9 nm, $\varepsilon = 8.64 \times 10^3$ L mol^{-1} cm^{-1}; ^{1}H NMR (400 MHz, $CDCl_3$): δ 16.63 (s, 3H, 3 × NH), 7.26 (s, 3H, Ar), 7.10 (dd, J_1 = 8.8 Hz, J_2 = 2.4 Hz, 3H, Ar), 6.91 (d, J = 8.8 Hz, 3H, Ar), 4.10 (m, 12H, 6 × OCH_2), 1.89−0.87 (m, 126H, 54 × CH_2, 6 × CH_3); ^{13}C NMR (100 MHz): 178.3, 150.5, 149.2, 135.2, 128.2, 113.9, 110.8, 102.7, 69.6, 69.5, 31.9, 29.6, 29.4, 29.3, 29.2, 26.1, 26.0, 22.7, 14.1. Anal. calcd for $C_{90}H_{150}N_6O_9$: C, 74.03; H, 10.35; N, 5.76; found: C, 73.94; H, 10.30; N, 5.76.

*2,4,6-Tris(2-(4-bis(3,4-dodecyloxy)phenyl)hydrazono)-cyclohexane-1,3,5-trione (**THN(6)12**).* A wine-red solid; yield: 0.123 g, 52%; IR (KBr pellet): ν_{max} in cm^{-1} 3474, 2924, 2855, 1589, 1469, 1230, 1122, 826; UV−vis: λ_{max} = 539.1 nm, $\varepsilon = 6.27 \times 10^3$ L mol^{-1} cm^{-1}; ^{1}H NMR (400 MHz, $CDCl_3$): δ 16.63 (s, 3H, 3 × NH), 7.26 (s, 3H, Ar), 7.10 (dd, J_1 = 8.8 Hz, J_2 = 2.4 Hz, 3H, Ar), 6.91 (d, J = 8.4 Hz, 3H, Ar), 4.12 (m, 12H, 6 × OCH_2), 1.87−0.86 (m, 138H, 60 × CH_2, 6 × CH_3); ^{13}C NMR (100 MHz): 178.3, 150.5, 149.2, 135.2, 128.2, 113.9, 110.7, 102.7, 69.6, 69.4, 31.9, 29.6, 29.4, 29.3, 29.2, 26, 22.7, 14.1. Anal. calcd for $C_{96}H_{162}N_6O_9$: C, 74.66; H, 10.57; N, 5.44; found: C, 74.57; H, 10.46; N, 5.46.

*2,4,6-Tris(2-(3,4-bis(((S)-3,7-dimethyloctyl)oxy)phenyl)-hydrazono)cyclohexane-1,3,5-trione (**THN-(6)10B**).* A wine-red gummy solid; yield: 0.101 g (48%); IR (KBr pellet): ν_{max} in cm^{-1} 3472, 2924, 2854, 1588, 1486, 1230, 1121, 824; UV−vis: λ_{max} = 536.4 nm, $\varepsilon = 4.40 \times 10^3$ L mol^{-1} cm^{-1}; ^{1}H NMR (400 MHz, $CDCl_3$): δ 16.58 (s, 3H, 3 × NH), 7.19 (s, 3H, Ar), 7.05 (dd, J_1 = 8.4 Hz, J_2 = 2.4 Hz, 3H, Ar), 6.85 (d, J = 8.8 Hz, 3H, Ar), 4.06 (m, 12H, 6 × OCH_2), 1.84−0.79 (m, 114H, 12 × CH, 24 × CH_2, 18 × CH_3); ^{13}C NMR (100 MHz): 178.4, 150.5, 149.2, 135.2, 128.2, 113.7, 110.7, 102.6, 67.9, 67.8, 39.3, 37.4, 36.2, 29.9, 28.0, 24.7, 22.7, 22.6, 19.7. Anal. calcd for $C_{84}H_{138}N_6O_9$: C, 73.32; H, 10.11; N, 6.11; found: C, 73.37; H, 10.08; N, 6.10.

*2,4,6-Tris(2-(3,4,5-tris(n-hexyloxy)phenyl)hydrazono)-cyclohexane-1,3,5-trione (**THN(9)6**).* A wine-red gummy solid; yield: 0.106 g, 52%; IR (KBr pellet): ν_{max} in cm^{-1} 3436, 2923, 2853, 1634, 1505, 1448, 1228, 1130, 820; UV−vis: λ_{max} = 534.2 nm, $\varepsilon = 3.68 \times 10^3$ L mol^{-1} cm^{-1}; ^{1}H NMR (400 MHz, $CDCl_3$): δ 16.49 (s, 3H, 3 × NH), 6.84 (s, 6H, Ar), 4.06 (m, 18H, 9 × OCH_2), 1.87−0.89 (m, 99H, 36 × CH_2, 9 × CH_3); ^{13}C NMR (100 MHz): 178.4, 154.2, 138.0, 136.8, 128.5, 96.3, 73.7, 69.3, 60.4, 31.7, 31.5, 30.3, 29.2, 25.7, 22.7,

https://dx.doi.org/10.1021/acsomega.0c05779
ACS Omega 2021, 6, 3291−3306

22.6, 14.1. Anal. calcd for $C_{78}H_{126}N_6O_{12}$: C, 69.92; H, 9.48; N, 6.27; found: C, 69.97; H, 9.55; N, 6.20.

*2,4,6-Tris(2-(3,4,5-tris(n-heptyloxy)phenyl)hydrazono)-cyclohexane-1,3,5-trione (**THN(9)7**)*. A wine-red gummy solid; yield: 0.121 g, 54%; IR (KBr pellet): ν_{max} in cm^{-1} 3438, 2924, 2854, 1633, 1487, 1228, 1127, 823; UV−vis: λ_{max} = 534.1 nm, $\varepsilon = 5.61 \times 10^3$ L mol $^{-1}$ cm^{-1}; ^{1}H NMR (400 MHz, $CDCl_3$): δ 16.49 (s, 3H, 3 × NH), 6.84 (s, 6H, Ar), 4.06 (m, 18H, 9 × OCH_2), 1.84−0.88 (m, 117H, 45 × CH_2, 9 × CH_3); ^{13}C NMR (100 MHz): 178.4, 154.2, 138.1, 136.8, 128.5, 96.4, 73.7, 69.4, 60.4, 31.9, 31.8, 30.9, 30.3, 29.7, 29.3, 29.2, 29.0, 26.0, 22.7, 22.6, 21.0, 14.1. Anal. calcd for $C_{87}H_{144}N_6O_{12}$: C, 71.27; H, 9.90; N, 5.73; found: C, 71.36; H, 9.98; N, 5.73.

*2,4,6-Tris(2-(3,4,5-tris(n-octyloxy)phenyl)hydrazono)-cyclohexane-1,3,5-trione (**THN(9)8**)*. A wine-red gummy solid; yield: 0.129 g, 53%; IR (KBr pellet): ν_{max} in cm^{-1} 3439, 2924, 2854, 1635, 1488, 1230, 1125, 821; UV−vis: λ_{max} = 536.0 nm, $\varepsilon = 3.98 \times 10^3$ L mol $^{-1}$ cm^{-1}; ^{1}H NMR (400 MHz, $CDCl_3$): δ 16.49 (s, 3H, 3 × NH), 6.84 (s, 6H, Ar), 4.10 (m, 18H, 9 × OCH_2), 1.87−0.88 (m, 135H, 54 × CH_2, 9 × CH_3); ^{13}C NMR (100 MHz): 178.4, 154.2, 138.1, 136.9, 96.4, 73.8, 69.4, 31.9, 31.8, 30.3, 29.5, 29.4, 29.3, 26.1, 22.7, 14.1. Anal. calcd for $C_{96}H_{162}N_6O_{12}$: C, 72.41; H, 10.25; N, 5.28; found: C, 72.31; H, 10.19; N, 5.33.

*2,4,6-Tris(2-(3,4,5-tris(n-nonyloxy)phenyl)hydrazono)-cyclohexane-1,3,5-trione (**THN(9)9**)*. A wine-red gummy solid; yield: 0.131 g, 50%; IR (KBr pellet): ν_{max} in cm^{-1} 3439, 2924, 2854, 1635, 1488, 1228, 1125,824; UV−vis: λ_{max} = 541.2 nm, $\varepsilon = 6.48 \times 10^3$ L mol $^{-1}$ cm^{-1}; ^{1}H NMR (400 MHz, $CDCl_3$): δ 16.48 (s, 3H, 3 × NH), 6.84 (s, 6H, Ar), 4.06 (m, 18H, 9 × OCH_2), 1.85−0.87 (m, 153H, 63 × CH_2, 9 × CH_3); ^{13}C NMR (100 MHz): 178.4, 154.2, 138.1, 136.8, 128.5, 96.3, 73.8, 69.4, 31.9, 30.3, 29.7, 29.6, 29.4, 29.3, 29.2, 26.1, 22.7, 14.1. Anal. calcd for $C_{105}H_{180}N_6O_{12}$: C, 73.38; H, 10.56; N, 4.89; found: C, 73.36; H, 10.43; N, 4.81.

*2,4,6-Tris(2-(3,4,5-tris(n-decyloxy)phenyl)hydrazono)-cyclohexane-1,3,5-trione (**THN(9)10**)*. A wine-red gummy solid; yield: 0.135 g, 48%; IR (KBr pellet): ν_{max} in cm^{-1} 3440, 2926, 2858, 1730, 1588, 1465, 1233, 1120, 831; UV−vis: λ_{max} = 535.0 nm, $\varepsilon = 4.38 \times 10^3$ L mol $^{-1}$ cm^{-1}; ^{1}H NMR (400 MHz, $CDCl_3$): δ 16.48 (s, 3H, 3 × NH), 6.84 (s, 6H, Ar), 4.06 (m, 18H, 9 × OCH_2), 1.85−0.87 (m, 171H, 72 × CH_2, 9 × CH_3); ^{13}C NMR (100 MHz): 178.4, 154.2, 138.1, 136.8, 128.5, 106.8, 96.4, 73.8, 69.4, 31.9, 30.3, 29.8, 29.7, 29.6, 29.4, 29.3, 26.1, 22.7, 14.1. Anal. calcd for $C_{114}H_{198}N_6O_{12}$: C, 74.22; H, 10.82; N, 4.56; found: C, 74.14; H, 10.89; N, 4.56.

*2,4,6-Tris(2-(3,4,5-tris(n-undecyloxy)phenyl)hydrazono)-cyclohexane-1,3,5-trione (**THN(9)11**)*. A wine-red gummy solid; yield: 0.136 g, 45%; IR (KBr pellet): ν_{max} in cm^{-1} 3441, 2926, 2857, 1730, 1588, 1466, 1233, 1121, 832; UV−vis: λ_{max} = 536.2 nm, $\varepsilon = 4.07 \times 10^3$ L mol $^{-1}$ cm^{-1}; ^{1}H NMR (400 MHz, $CDCl_3$): δ 16.49 (s, 3H, 3 × NH), 6.84 (s, 6H, Ar), 4.06 (m, 18H, 9 × OCH_2), 1.85−0.86 (m, 189H, 81 × CH_2, 9 × CH_3); ^{13}C NMR (100 MHz): 178.4, 154.2, 138.1, 136.8, 128.5, 96.4, 73.8, 69.4, 31.9, 30.4, 29.7, 29.6, 29.4, 26.1, 22.7, 14.1. Anal. calcd for $C_{123}H_{216}N_6O_{12}$: C, 74.95; H, 11.05; N, 4.26; found: C, 74.87; H, 11.03; N, 4.24.

*2,4,6-Tris(2-(3,4,5-tris(n-dodecyloxy)phenyl)hydrazono)-cyclohexane-1,3,5-trione (**THN(9)12**)*. A wine-red gummy solid; yield: 0.128 g, 40%; IR (KBr pellet): ν_{max} in cm^{-1} 3496, 2923, 2854, 1589, 1451, 1231, 1125, 826; UV−vis: λ_{max} = 536.2 nm, $\varepsilon = 4.28 \times 10^3$ L mol $^{-1}$ cm^{-1}; ^{1}H NMR (400 MHz, $CDCl_3$): δ 16.48 (s, 3H, 3 × NH), 6.84 (s, 6H, Ar), 4.06 (m, 18H, 9 × OCH_2), 1.85−0.86 (m, 207H, 90 × CH_2, 9 × CH_3); ^{13}C NMR (100 MHz): 178.4, 154.2, 138.1, 136.8, 128.5, 106.8, 96.4, 73.7, 69.4, 31.9, 30.3, 29.8, 29.7, 29.6, 29.4, 29.3, 26.1, 22.7, 14.1. Anal. calcd for $C_{132}H_{234}N_6O_{12}$: C, 75.59; H, 11.25; N, 4.01; found: C, 75.60; H, 11.27; N, 4.00.

*2,4,6-Tris(2-(3,4,5-tris(((S)-3,7-dimethyloctyl)oxy)phenyl)-hydrazono)cyclohexane-1,3,5-trione (**THN(9)10B**)*. A wine-red gummy solid; yield: 0.127 g, 45%; IR (KBr pellet): ν_{max} in cm^{-1} 3440, 2926, 2858, 1730, 1588, 1466, 1233, 1121, 832; UV−vis: λ_{max} = 536.8 nm, $\varepsilon = 2.96 \times 10^3$ L mol $^{-1}$ cm^{-1}; ^{1}H NMR (400 MHz, $CDCl_3$): δ 16.52 (s, 3H, 3 × NH), 6.85 (s, 6H, Ar), 4.12 (m, 18H, 9 × OCH_2), 1.92−0.86 (m, 171H, 18 × CH, 36 × CH_2, 27 × CH_3); ^{13}C NMR (100 MHz): 178.4, 154.2, 138.1, 136.9, 128.5, 96.4, 72.0, 67.7, 39.4, 39.3, 37.5, 37.4, 36.4, 29.8, 29.7, 28.0, 24.7, 22.7, 22.6, 19.6. Anal. calcd for $C_{114}H_{198}N_6O_{12}$: C, 74.22; H, 10.82; N, 4.56; found: C, 74.15; H, 10.82; N, 4.50.

■ ASSOCIATED CONTENT

Supporting Information

The Supporting Information is available free of charge at https://pubs.acs.org/doi/10.1021/acsomega.0c05779.

^{1}H and ^{13}C NMR spectra; TGA graphs; textural photomicrographs; DSC thermograms; powder XRD patterns; UV−vis and emission spectra; quantum yield; profiles of integrated fluorescence intensity vs the absorbance (PDF)

■ AUTHOR INFORMATION

Corresponding Author

Channabasaveshwar V. Yelamaggad − *Centre for Nano and Soft Matter Sciences, Bangalore 560013, India;* orcid.org/0000-0003-3098-8358; Email: yelamaggad@cens.res.in, yelamaggad@gmail.com

Authors

Rashmi Ashwathama Nayak − *Centre for Nano and Soft Matter Sciences, Bangalore 560013, India*

Bhyranalyar Nagarajappa Veerabhadraswamy − *Centre for Nano and Soft Matter Sciences, Bangalore 560013, India*

Doddamane S. Shankar Rao − *Centre for Nano and Soft Matter Sciences, Bangalore 560013, India;* orcid.org/0000-0002-9643-6604

Achalkumar Ammathnadu Sudhakar − *Department of Chemistry, Indian Institute of Technology Guwahati, Guwahati 781039, India;* orcid.org/0000-0003-4952-9450

Complete contact information is available at: https://pubs.acs.org/10.1021/acsomega.0c05779

Notes

The authors declare no competing financial interest.

■ ACKNOWLEDGMENTS

C.V.Y. profoundly thanks and sincerely acknowledges the financial support from Science and Engineering Research Board (SERB), Department of Science and Technology (DST), Government of India, under Project No. EMR/2017/ 000153.

REFERENCES

(1) Zhao, J.; Zhong, D.; Zhou, S. NIR-I-to-NIR-II fluorescent nanomaterials for biomedical imaging and cancer therapy. *J. Mater. Chem. B* **2018**, *6*, 349−365.

(2) Kono, M.; Ueki, H.; Umemura, S.-I. Near-infrared finger vein patterns for personal identification. *Appl. Opt.* **2002**, *41*, No. 7429.

(3) Zampetti, A.; Minotto, A.; Cacialli, F. Near-Infrared (NIR) Organic Light-Emitting Diodes (OLEDs): Challenges and Opportunities. *Adv. Funct. Mater.* **2019**, *29*, No. 1807623.

(4) Xu, T.; Yu, L. How to design low bandgap polymers for highly efficient organic solar cells. *Mater. Today* **2014**, *17*, 11−15.

(5) Shirota, Y. Organic materials for electronic and optoelectronic devices. *J. Mater. Chem.* **2000**, *10*, 1−25.

(6) Kalyani, N. T.; Dhoble, S. J. Organic light emitting diodes: Energy saving lighting technology—A review. *Renewable Sustainable Energy Rev.* **2012**, *16*, 2696−2723.

(7) Kido, J.; Kimura, M.; Nagai, K. Multilayer White Light-Emitting Organic Electroluminescent Device. *Science* **1995**, *267*, 1332−1334.

(8) Gather, M. C.; Kohnen, A.; Meerholz, K. White Organic Light-Emitting Diodes. *Adv. Mater.* **2011**, *23*, 233.

(9) D'Andrade, B. W.; Holmes, R. J.; Forrest, S. R. White Organic Light-Emitting Devices for Solid-State Lighting. *Adv. Mater.* **2004**, *16*, 1585−1595.

(10) Bisoyi, H. K.; Li, Q. Stimuli directed alignment of self-organized one-dimensional semiconducting columnar liquid crystal nanostructures for organic electronics. *Prog. Mater. Sci.* **2019**, *104*, 1−52.

(11) Wöhrle, T.; Wurzbach, I.; Kirres, J.; Kostidou, A.; Kapernaum, N.; Litterscheidt, J.; Haenle, J. C.; Staffeld, P.; Baro, A.; Giesselmann, F.; Laschat, S. Discotic Liquid Crystals. *Chem. Rev.* **2016**, *116*, 1139−1241.

(12) Chong, J. H.; Sauer, M.; Patrick, B. O.; MacLachlan, M. J. Highly stable Keto-enamine salicylidene-anilines. *Org. Lett.* **2003**, *21*, No. 3823.

(13) Yelamaggad, C. V.; Achalkumar, A. S.; Rao, D. S. S.; Prasad, S. K. A New Class of Discotic Mesogens Derived from Tris(*N*-salicylideneaniline)s Existing in C_{3h} and C_s Keto-Enamine Forms. *J. Org. Chem.* **2007**, *72*, 8308−8318.

(14) Yelamaggad, C. V.; Achalkumar, A. S.; Rao, D. S. S.; Prasad, S. K. The first examples of optically active tris(*N*-salicylideneaniline)s: manifestation of chirality from molecules to fluid columnar phases. *J. Mater. Chem.* **2007**, *17*, 4521−4529.

(15) Yelamaggad, C. V.; Achalkumar, A. S.; Rao, D. S. S.; Prasad, S. K. Luminescent, Liquid Crystalline Tris(*N*-salicylideneaniline)s: Synthesis and Characterization. *J. Org. Chem.* **2009**, *74*, 3168−3171.

(16) Yelamaggad, C. V.; Achalkumar, A. S. Light emitting, star-shaped tris(N-salicylideneaniline) discotic liquid crystals bearing trans-stilbene fluorophores: synthesis and characterization. *Tetrahedron Lett.* **2012**, *53*, 7108−7112.

(17) Achalkumar, A. S.; Hiremath, U. S.; Rao, D. S. S.; Prasad, S. K.; Yelamaggad, C. V. Self-Assembly of Hekates-Tris(N-salicylideneaniline)s into Columnar Structures: Synthesis and Characterization. *J. Org. Chem.* **2013**, *78*, 527−544.

(18) Achalkumar, A. S.; Veerabhadraswamy, B. N.; Hiremath, U. S.; Rao, D. S. S.; Prasad, S. K.; Yelamaggad, C. V. Photoluminescent discotic liquid crystals derived from tris(N-salicylideneaniline) and stilbene conjugates: Structure property correlations. *Dyes Pigm.* **2016**, *132*, 291−305.

(19) Pathak, S. K.; Nath, S.; De, J.; Pal, S. K.; Achalkumar, A. S. Contrasting effects of heterocycle substitution and branched tails in the arms of star-shaped molecules. *New J. Chem.* **2017**, *41*, 4680−4688.

(20) Pathak, S. K.; Nath, S.; De, J.; Pal, S. K.; Achalkumar, A. S. The effect of regioisomerism on the mesomorphic and photophysical behavior of oxadiazole-based tris(N-salicylideneaniline)s: synthesis and characterization. *New J. Chem.* **2017**, *41*, 9908−9917.

(21) Gupta, R. K.; Pathak, S. K.; De, J.; Pal, S. K.; Achalkumar, A. S. Room temperature columnar liquid crystalline self-assembly of acidochromic, luminescent, star-shaped molecules with cyanovinylene chromophores. *J. Mater. Chem. C* **2018**, *6*, 1844−1852.

(22) Lee, H. Y.; Song, X.; Park, H.; Baik, M.-H.; Lee, D. Torsionally responsive C3-symmetric azo dyes: azo-hydrazone tautomerism, conformational switching, and application for chemical sensing. *J. Am. Chem. Soc.* **2010**, *132*, 12133−12144.

(23) Li, X.; Liu, A.; Xun, S.; Qiao, W.; Wan, X.; Wang, Z. Y. Synthesis and Characterization of Near-Infrared Absorbing and Fluorescent Liquid-Crystal Chromophores. *Org. Lett.* **2008**, *10*, 3785−3787.

(24) Liu, C.; Ding, W.; Liu, Y.; Zhao, H.; Cheng, X. Self-assembled star-shaped aza-BODIPY mesogen affords white-light emission. *New J. Chem.* **2020**, *44*, 102−109.

(25) Hayer, A.; de Halleux, V.; Kohler, A.; El-Garoughy, A.; Meijer, E. W.; Barbera, J.; Tant, J.; Levin, J.; Lehmann, M.; Gierschner, J.; Cornil, J.; Geerts, Y. H. *J. Phys. Chem. B.* **2006**, *110*, 7653.

(26) Wicklein, A.; Muth, M.-A.; Thelakkat, M. Room temperature liquid crystalline perylene diester benzimidazoles with extended absorption. *J. Mater. Chem.* **2010**, *20*, 8646.

(27) Fang, X.; Guo, H.; Yang, F.; Lin, J. Near-infrared fluorescent and columnar liquid crystal: synthesis, and photophysical and mesomorphic properties of triphenylene-Bodipy- triphenylene triad. *RSC Adv.* **2017**, *7*, 23657−23662.

(28) Laschat, S.; Baro, A.; Steinke, N.; Giesselmann, F.; Hägele, C.; Scalia, G.; Judele, R.; Kapatsina, E.; Sauer, S.; Schreivogel, A.; Tosoni, M. Discotic Liquid Crystals: From Tailor-Made Synthesis to Plastic Electronics. *Angew. Chem., Int. Ed.* **2007**, *46*, 4832−4887.

(29) Do, T. H.; Kim, H.-J.; Nguyen, M. L.; Cho, B.-K. Bicontinuous Cubic and Hexagonal Columnar Liquid Crystalline Ion-Conductors at Room Temperature in Ion-Doped Dendritic Amphiphiles. *Crystals* **2020**, *10*, 1−12.

(30) Shimizu, M.; Hiyama, T. Organic fluorophores exhibiting highly efficient photoluminescence in the solid state. *Chem.- Asian J.* **2010**, *5*, 1516−1531.

(31) Grimsdale, A. C.; Chan, K. L.; Martin, R. E.; Jokisz, P. G.; Holmes, A. B. Synthesis of light-emitting conjugated polymers for applications in electroluminescent devices. *Chem. Rev.* **2009**, *109*, 897−1091.

(32) Liu, J. Z.; Lam, J. W. Y.; Tang, B. Z. Acetylenic polymers: syntheses, structures, and functions. *Chem. Rev.* **2009**, *109*, 5799−5867.

(33) Prabhu, D. D.; Kumar, N. S. S.; Sivadas, A. P.; Varghese, S.; Das, S. Trigonal 1, 3, 4-oxadiazole-based blue-emitting liquid crystals and gels. *J. Phys. Chem. B* **2012**, *116*, 13071−13080.

https://dx.doi.org/10.1021/acsomega.0c05779
ACS Omega 2021, 6, 3291−3306